Article

Cell Reports

TETs Regulate Proepicardial Cell Migration through Extracellular Matrix Organization during Zebrafish Cardiogenesis

Graphical Abstract

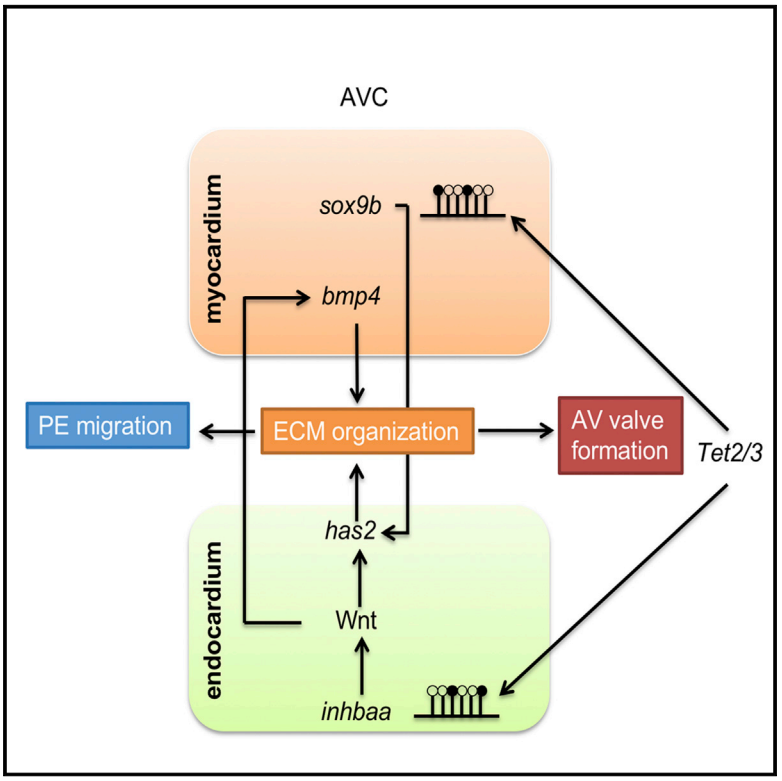

Authors

Yahui Lan, Heng Pan, Cheng Li, ..., Olivier Elemento, Mary G. Goll, Todd Evans

Correspondence

tre2003@med.cornell.edu

In Brief

Lan et al. show that zebrafish larvae mutant for *tet2* and *tet3* fail to demethylate genes encoding Inhbaa (in endocardium) and Sox9b (in myocardium), leading to defects in ECM needed to form valves and to recruit epicardial progenitors onto the heart tube.

Highlights

- Zebrafish larvae lacking Tet2 and Tet3 fail in AVC and epicardium development
- Inhbaa (in endocardium) and Sox9b (in myocardium) are targets of Tet2/3 demethylation
- These genes help coordinate ECM needed by epicardial progenitors

Lan et al., 2019, Cell Reports *26*, 720–732
January 15, 2019
https://doi.org/10.1016/j.celrep.2018.12.076

CellPress

OPEN ACCESS
CellPress

Cell Reports
Article

TETs Regulate Proepicardial Cell Migration through Extracellular Matrix Organization during Zebrafish Cardiogenesis

Yahui Lan,[1] Heng Pan,[2] Cheng Li,[3,4] Kelly M. Banks,[1] Jessica Sam,[1] Bo Ding,[5] Olivier Elemento,[2] Mary G. Goll,[3,6] and Todd Evans[1,7,*]

[1]Department of Surgery, Weill Cornell Medical College, New York, NY 10065, USA
[2]Department of Physiology and Biophysics, Englander Institute for Precision Medicine, Institute for Computational Biomedicine, Weill Cornell Medical College, New York, NY 10065, USA
[3]Developmental Biology Program, Memorial Sloan Kettering Cancer Center, New York, NY 10065, USA
[4]Program in Biochemistry and Structural Biology, Cell and Developmental Biology, and Molecular Biology, Weill Cornell Graduate School of Medical Sciences, Cornell University, New York, NY 10065, USA
[5]Bonacept, LLC, 7699 Palmilla Drive, Apt. 3312, San Diego, CA 92122, USA
[6]Present address: Department of Genetics, University of Georgia, Athens, GA 30602, USA
[7]Lead Contact
*Correspondence: tre2003@med.cornell.edu
https://doi.org/10.1016/j.celrep.2018.12.076

SUMMARY

Ten-eleven translocation (Tet) enzymes (Tet1/2/3) mediate 5-methylcytosine (5mC) hydroxylation, which can facilitate DNA demethylation and thereby impact gene expression. Studied mostly for how mutant isoforms impact cancer, the normal roles for Tet enzymes during organogenesis are largely unknown. By analyzing compound mutant zebrafish, we discovered a requirement for Tet2/3 activity in the embryonic heart for recruitment of epicardial progenitors, associated with development of the atrial-ventricular canal (AVC). Through a combination of methylation, hydroxymethylation, and transcript profiling, the genes encoding the activin A subunit Inhbaa (in endocardium) and Sox9b (in myocardium) were implicated as demethylation targets of Tet2/3 and critical for organization of AVC-localized extracellular matrix (ECM), facilitating migration of epicardial progenitors onto the developing heart tube. This study elucidates essential DNA demethylation modifications that govern gene expression changes during cardiac development with striking temporal and lineage specificities, highlighting complex interactions in multiple cell populations during development of the vertebrate heart.

INTRODUCTION

Epigenetics refers to heritable changes in gene expression without DNA sequence alteration. Epigenetic modifications, including histone phosphorylation and methylation and DNA methylation and demethylation, can alter DNA accessibility and chromatin structure, thereby regulating gene expression (Loscalzo and Handy, 2014). In vertebrates, DNA methylation at the 5 position of cytosine (5mC) is often associated with transcriptional repression and is one of the key epigenetic mechanisms used during normal development (Goll and Bestor, 2005); alteration in DNA methylation patterns has been implicated in various disease states (Robertson, 2005). The mechanisms that establish and maintain 5mC are well defined, including *de novo* methylation through DNA methyltransferase-3 (Dnmt3) family proteins and maintenance methylation by Dnmt1 (Hu et al., 2012; Feng et al., 2010; Sen et al., 2010). Blocking the action of maintenance methylation leads to passive loss of 5mC through dilution of marks in replicating cells. However, there is good evidence that methyl marks can be actively removed, even in the absence of DNA replication (Wu and Zhang, 2017).

Recent studies identified the ten-eleven translocation (TET) proteins TET1, TET2, and TET3 as a family of 2-oxoglutarate- and Fe(II)-dependent dioxygenases that alter the methylation status of DNA by converting 5mC to 5-hydroxymethylcytosine (5hmC) and then 5-formylcytosine (5fC) and 5-carboxylcytosine (5caC), followed by replication-dependent dilution or thymine DNA glycosylase (TDG)-dependent base excision repair (He et al., 2011; Wu and Zhang, 2011; Pastor et al., 2013). Defects in this pathway are associated with multiple diseases, including cancer. Mutations in *TET* genes, most notably *TET2*, are associated with human hematopoietic malignancies (Ko et al., 2015; Madzo et al., 2014) and more recently are implicated in clonal hematopoiesis associated with risk for leukemia and cardiovascular disease (Solary et al., 2014; Turgeon et al., 2014). Animal and cell models have tested the impact of losing TET activity. *Tet3* knockout mice die perinatally (Kohli and Zhang, 2013). Although *Tet1* and *Tet2* mutant mice are viable and fertile, half of *Tet1*$^{-/-}$; *Tet2*$^{-/-}$ double null embryos exhibit midgestation abnormalities with perinatal lethality (Dawlaty et al., 2013). Both mouse and human embryonic stem cells (ESCs) carrying null mutations for all three *Tet* genes show impaired ability to differentiate and contribute poorly to teratomas or chimeras (Verma et al., 2018;

Dawlaty et al., 2014). We (Li et al., 2015) and others (Seritrakul and Gross, 2017) reported overlapping requirements for *tet2* and *tet3* during zebrafish hematopoietic stem cell emergence and retinal neurogenesis, respectively. Less is known about specific requirements for *TET* genes during organogenesis and morphogenesis. DNA hydroxymethylation is associated with myocardial gene expression in maturation and hypertrophy (Kranzhöfer et al., 2016; Greco et al., 2016), suggesting that *TET* genes might be required during cardiogenesis.

The vertebrate heart forms from progenitor cells derived from multiple, distinct embryonic origins (Meilhac et al., 2004). The primitive heart tube forms from first-heart-field-derived mesoderm that generates myocardium associated with the underlying endocardium to form a beating heart tube. The atrial-ventricular canal (AVC) forms by repression of the muscle program to distinguish the primitive atrial and ventricular chambers and formation of cushions preceding valvulogenesis. Second heart field mesoderm adds to both the venous and arterial poles during formation of inflow and outflow tracts, respectively. Additional progenitors migrate to form an extracardiac rudiment called the proepicardium (PE) (comprising epicardial progenitors). Once the PE attaches to the heart, it undergoes morphogenesis to form an epithelial covering called epicardium, which is the source of cardiac pericytes and vascular smooth muscle cells and also acts as a sleeve, allowing ingrowth of the microvasculature (Chen et al., 2014; Dettman et al., 1998; Lindsey et al., 2014; Peralta et al., 2014; Poelmann et al., 1993; Ratajska et al., 2008; Red-Horse et al., 2010; Snarr et al., 2008). Here, we describe a combined requirement for Tet2 and Tet3 in facilitating zebrafish PE attachment. The results highlight exquisite spatial and temporal control of DNA methylation patterns underlying complex interactions of cell populations during cardiac morphogenesis.

RESULTS

Overlapping Requirement for Tet2 and Tet3 in PE Morphogenesis

Loss of any single *tet1/2/3* gene is tolerated in zebrafish embryos and adults. By combining mutant alleles, we showed previously that Tet2 and Tet3 are the major 5mC dioxygenases in the zebrafish embryo and that most hydroxymethylation is lost in the double mutant embryos, associated with developmental defects, including a failure to generate hematopoietic stem cells, neural defects, and pericardial edema (Li et al., 2015), the latter of which indicates potential functions during cardiogenesis. Specification of cardiac progenitors and formation of a primitive heart tube was normal in *tet2* and *tet3* double homozygous mutant (*tet2/3*^{DM}) larvae, assessed by expression patterns of *gata4*, *nkx2.5*, *myh6*, and *myh7* using whole-mount *in situ* hybridization (WISH) (Figure S1A). RNA sequencing data at 28 h post-fertilization (hpf) indicated neural developmental defects in *tet2/3*^{DM} larvae (Figure S1B). In contrast, an equivalent cardiac transcriptomic profile was found comparing *tet2/3*^{DM} and wild-type or sibling larvae (Figure S1C), consistent with normal early heart development. Imaging of *tet2/3*^{DM} larvae in the background of fluorescent reporter strains showed that endocardial marker *kdrl* and myocardial marker *myl7* were grossly normal during the first 2 days of development (Figures S2A–S2F). The mutant hearts beat and normal expression of *klf2a* (an immediate early responder to flow) suggest that blood flow is also grossly normal during the first 2 days of development (Li et al., 2015). This was confirmed by directly measuring heart rate, which did not differ significantly comparing sibling and mutant embryos (Figure S2G). Although expression of PE marker *wt1* was also normal at 40 hpf, *wt1* expression patterns were reduced and restricted at 54 hpf in *tet2/3*^{DM} larvae compared to stage-matched sibling controls (Figure 1A), suggesting a defect in epicardial development.

To further evaluate epicardial development in *tet2/3*^{DM} larvae, the mutant alleles were crossed onto the *Tg(tcf21:NLS-EGFP)* transgenic background, in which GFP is expressed in PE as well as epicardium (Figure 1B). Consistent with previous findings (Plavicki et al., 2014b), in sibling larvae, PE were observed near the heart at 46 hpf and found attaching to the heart around the atrioventricular (AV) junction at 52 hpf. By 72 hpf, in addition to the establishment of epicardial cells on the ventricle, a bridge can be seen between the AV junction and pericardium as a path for PE cells migrating onto the heart. Although PE could be found in the pericardial region at 46 hpf in *tet2/3*^{DM} larvae, they failed to attach to or migrate onto the heart at 52 hpf or 72 hpf (Figure 1B), suggesting a PE morphogenesis defect in *tet2/3*^{DM} larvae. To clarify whether this was a migration or proliferation defect, we quantified *tcf21*+ PE cell numbers and found a similar number of PE cells in sibling or *tet2/3*^{DM} larvae at 48 hpf (Figure 1C). By 72 hpf, the total number of *tcf21*+ PE cells was not different comparing siblings and *tet2/3*^{DM} larvae. However, in *tet2/3*^{DM} larvae, the cells failed to migrate to the ventricle and accumulated in the pericardial region, indicated by increased numbers of *tcf21*+ cells on the yolk sac of *tet2/3*^{DM} larvae (Figure 1C). Moreover, pH3 antibody staining suggested essentially no cell proliferation of *tcf21*+ PE cells at 48 hpf or 72 hpf (Figure S3). Therefore, in *tet2/3*^{DM} larvae, there is normal specification and no impact on proliferation but rather a marked defect in migration during PE morphogenesis.

To validate that the phenotype was caused by loss of Tet function and specifically DNA demethylation, we attempted to rescue PE migration in *tet2/3*^{DM} larvae by forced *TET* expression or by inhibiting DNA methylation. Embryos derived from *tet2*$^{-/-}$*tet3*$^{+/-}$ intercrosses were injected with *in vitro* transcribed mRNA encoding human TET2 at the one-cell stage or cultured in the presence of the DNA methyltransferase inhibitor 5-aza-2′-deoxycytidine (5-aza) from 24 hpf. The number of *tcf21*+ epicardial cells associated with the developing ventricle was subsequently examined in *tet2/3*^{DM} larvae by confocal imaging at 4 dpf. Either strategy partially rescued the PE migration and morphogenesis defect in *tet2/3*^{DM} larvae (Figure 1D). Moreover, injection of mRNA encoding a catalytically dead version of TET2 failed to rescue PE migration, directly implicating a critical function for *tet2* and *tet3* in regulating PE migration through DNA demethylation.

Tet2 and Tet3 Regulate PE Migration by Modulating Myocardial Function

An *in vitro* epicardial migration assay was performed to test whether the PE migration defect in *tet2/3*^{DM} larvae is cell autonomous or non-cell autonomous for epicardium (Figure 2A). In the assay, donor hearts were isolated from embryos transgenic for

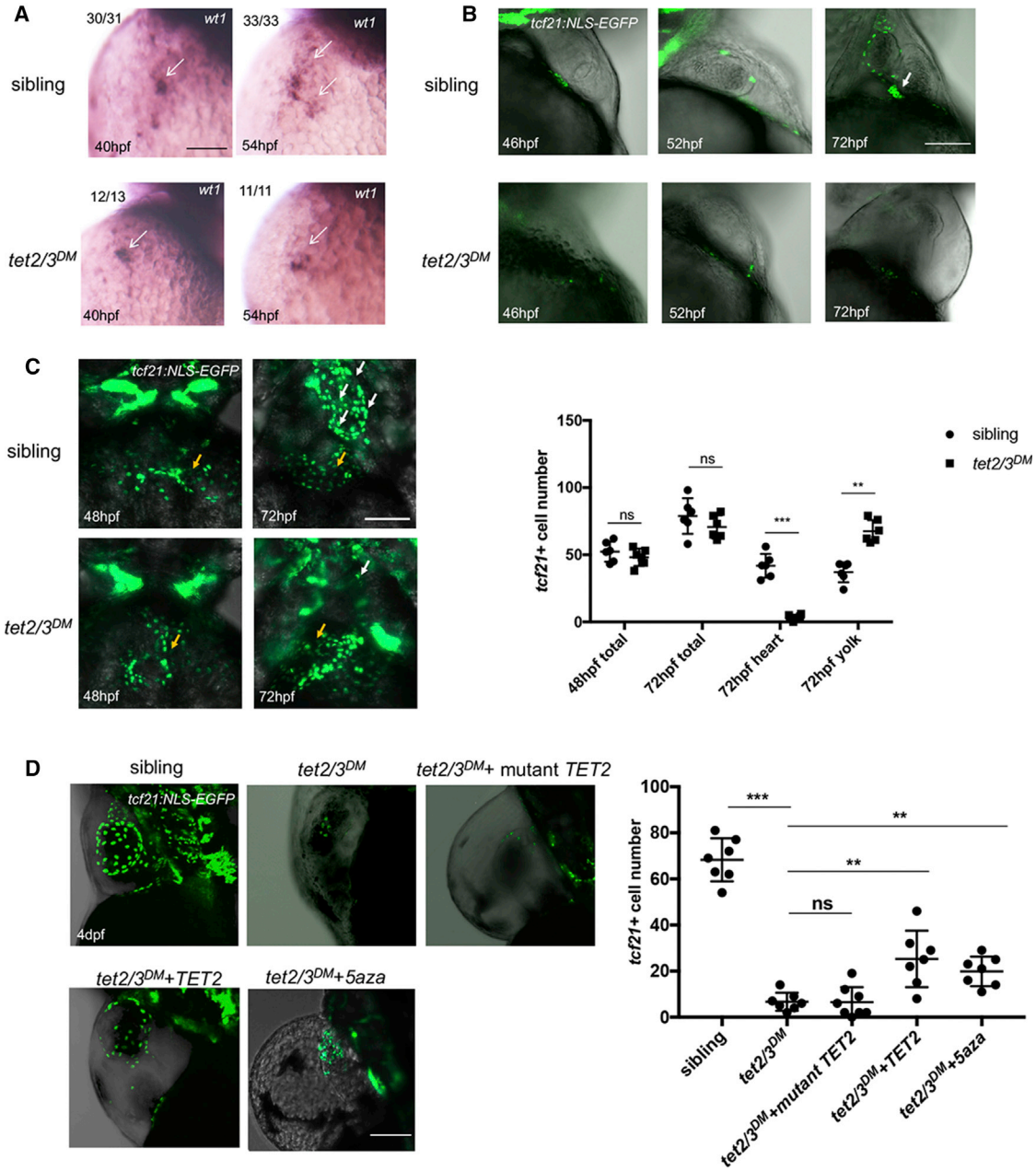

Figure 1. *tet2* and *tet3* Have Overlapping Functions in PE Recruitment to the Heart

(A) WISH for PE marker *wt1* at 40 hpf and 54 hpf. Arrows indicate PE cells with *wt1* transcripts.

(B) Lateral view of hearts showing GFP-labeled PE and epicardium in 46-hpf, 52-hpf, and 72-hpf larvae carrying the Tg(*tcf21:NLS-EGFP*) transgene. White arrow indicates the extracellular matrix bridge between AVC and the pericardial wall.

(C) Ventral view of hearts showing GFP-labeled PE and epicardium in 48-hpf and 72-hpf sibling or *tet2/3*^{DM} larvae carrying the Tg(*tcf21:NLS-EGFP*) transgene. White arrows indicate *tcf21*+ PE and epicardial cells located on the heart. Yellow arrows indicate *tcf21*+ PE and epicardial cells located on the yolk sac. Graph indicates the total number of PE and epicardial cells in 48-hpf or 72-hpf sibling and *tet2/3*^{DM} larvae and the number of PE and epicardial cells located on heart or yolk sac at 72-hpf sibling and *tet2/3*^{DM} larvae.

(D) The PE migration defect is partially rescued by TET2 mRNA injection or 5-aza treatment. GFP-labeled PE and epicardium in 4-dpf sibling, *tet2/3*^{DM}, and *tet2/3*^{DM} injected with wild-type hTET2 mRNA, mutant hTET2 mRNA, or *tet2/3*^{DM} exposed to 75 μM 5-aza larvae carrying the Tg(*tcf21:NLS-EGFP*) transgene. Graph indicating the number of epicardial cells located on the heart at 4 dpf is shown.

Scale bars: (A) 50 μm; (B–D) 100 μm. **p < 0.01; ***p < 0.001; ns indicates not significant. Data are presented as mean ± SD derived from at least three independent biological replicates.

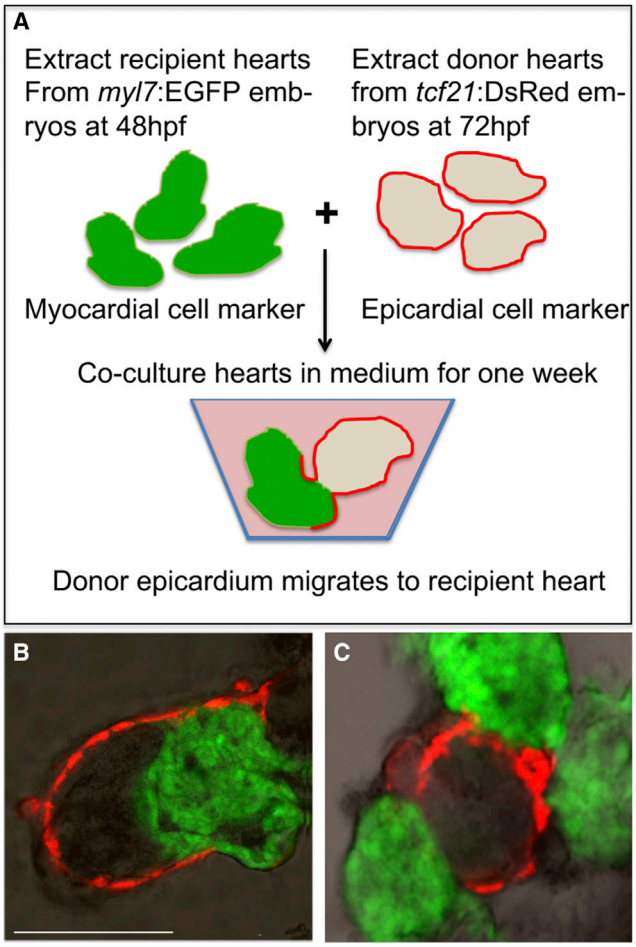

Figure 2. Epicardial Cells from Donor Hearts Do Not Migrate onto *tet2/3*^{DM} Recipient Hearts

(A) Schematic of epicardial cell migration assay. Wild-type *tcf21*:DsRed donor hearts (isolated at 72 hpf) were co-cultured with either wild-type or *tet2/3*^{DM} *myl7*:GFP recipient hearts (isolated at 48 hpf) for one week and then confocal images taken.

(B) Confocal images showed epicardial cells from wild-type donor heart can migrate onto wild-type recipient hearts. In 30 pairs of co-cultured hearts, 6 of recipient hearts were observed having epicardial cells migrated from donor hearts.

(C) Confocal images showed epicardial cells from wild-type donor heart failed to migrate onto *tet2/3*^{DM} recipient hearts. In 60 pairs of co-cultured hearts, none of the recipient hearts were observed having epicardial cells from donor hearts.

Scale bar: 50 μm.

the Tg(*tcf21:DsRed*) epicardial cell reporter at 72 hpf, and recipient hearts were isolated from embryos transgenic for the Tg(*myl7:EGFP*) myocardial reporter at 48 hpf, before epicardial cells had migrated onto the myocardium. After a week of co-culture, epicardial cells from wild-type donor hearts could be observed covering wild-type recipient hearts (Figure 2B). However, epicardial cells from wild-type donor hearts failed to migrate onto *tet2/3*^{DM} recipient hearts (Figure 2C), demonstrating a non-cell autonomous role for Tet2/3 in epicardial cell migration. Because the recipient experiment could not be performed due to a lack of epicardium in *tet2/3*^{DM} hearts, a cell-autonomous role for Tet2/3 could not be evaluated. Overall, our data suggest that myocardial Tet2/3 is required for promoting PE migration during cardiac development.

Deficiency of Tet Activity Leads to Hypermethylation and Deregulation of Developmental Genes during Cardiogenesis

Because *tet2* and *tet3* appear to regulate epicardium at least in part through a non-cell-autonomous fashion, we sought to identify potential factors responsible for these effects, utilizing both methylomic and transcriptomic analyses. The developing *tet2/3*^{DM} larvae are largely depleted of 5hmC (Li et al., 2015), so it was important to first map the normal distribution of 5hmC sites. For this purpose, 5hMe-bead-integrated click-seq (5hMe-BIC-seq) was performed using genomic DNA from wild-type 48 hpf hearts. We identified 145,501 5hmC-occupied peaks and defined the distribution of these peaks in the zebrafish genome in four regions: promoters (2 kb upstream and downstream of transcription start sites); active enhancers (peaks overlapped with H3K4me1 and H3K27ac peaks, but not overlapped with promoters or exons); poised enhancers (peaks overlapped with H3K4me1 peaks only, but not overlapped with H3K27ac peaks, promoters, or exons); and other regions. The majority (over 60%) of 5hmC-associated regions were found in active enhancers, with another 5% mapping to transcriptional regulatory regions, including promoters and poised enhancers (Figure 3A), which is consistent with previous mouse and zebrafish data (Bogdanović et al., 2016; Hon et al., 2014).

To determine the impact of Tet enzyme loss and 5hmC depletion on DNA methylation, hearts from wild-type or *tet2/3*^{DM} larvae were isolated at 48 hpf and ERRBS (enhanced reduced representation bisulfite sequencing) was performed to compare their 5mC profiles. In *tet2/3*^{DM} heart tissue, a total of 10,494 differentially methylated regions were found with increased methylation (hyper-differentially methylated regions [DMRs]), and much fewer, only 829, showed decreased methylation (hypo-DMRs; Figure 3B), which is consistent with a function for Tet enzymes in DNA demethylation. Hyper-DMRs in the mutant hearts showed a distribution pattern similar to 5hmC in the wild-type embryos, specifically enriched in active enhancers and other regulatory regions (Figure 3A). Moreover, most hyper-DMRs in mutants co-localized with 5hmC peaks in wild-type (Figure 3C), demonstrating the close association of 5hmC during DNA demethylation. Gene pathway analysis of these hyper-DMR-associated genes showed a significant enrichment for developmental signaling pathways, including Notch, Wnt, transforming growth factor β (TGF-β), and bone morphogenetic protein (BMP) pathways (Figure 3D). Notably, these pathways are all highly associated with cardiac development (Azhar et al., 2003; Wang et al., 2013), suggesting that Tet2/3-mediated DNA demethylation regulates important signaling functions during cardiogenesis.

To investigate the transcriptional consequences of these methylation changes, RNA sequencing (RNA-seq) was also performed using isolated wild-type and *tet2/3*^{DM} hearts at 48 hpf. In the *tet2/3*^{DM} hearts, 129 genes were downregulated and 160 genes were upregulated (Figure 3E). For a select subset of top differentially expressed genes, qPCR analysis confirmed

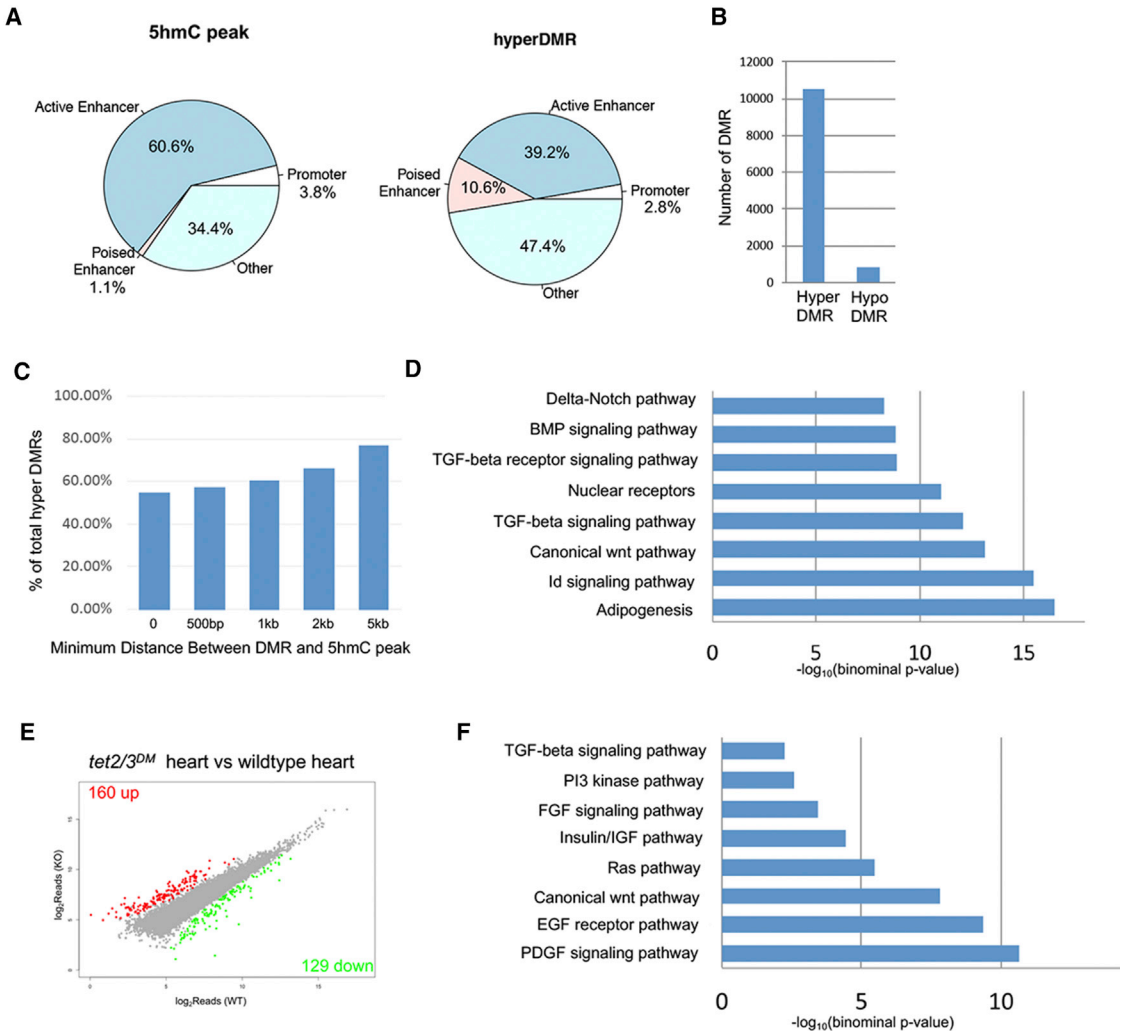

Figure 3. Hypermethylation and Deregulation of Cardiac Developmental Genes in *tet2/3*^{DM} Larvae

(A) Enrichment of various regulatory regions in 5hmC peak and hyper-DMR by 5hmC chromatin immunoprecipitation (ChIP)-sequencing and ERRBS.

(B) Total number of hyper- and hypo-DMR (*tet2/3*^{DM} heart versus wild-type heart) by ERRBS.

(C) Overlapping locations between hyper-DMRs and 5hmC peaks.

(D) Pathway enrichment analysis for genes associated with hyper-DMR.

(E) Scatterplot of RNA sequencing data illustrating transcriptional changes in 48-hpf *tet2/3*^{DM} heart as compared to wild-type heart.

(F) Pathway enrichment analysis for downregulated genes in 48-hpf *tet2/3*^{DM} heart as compared to wild-type heart by RNA sequencing.

cardiac transcriptional alterations in *tet2/3*^{DM} hearts, compared with sibling or wild-type hearts. Interestingly, these differences were not found in samples generated from whole embryos, demonstrating the requirement to isolate heart tissue to reveal cardiac-specific gene regulation changes (Figure S4A). Gene Ontology (GO) analysis suggested that downregulated genes in *tet2/3*^{DM} mutant hearts are involved in heart morphogenesis, vasculature development, cell motility and junction, and muscle differentiation (Figure S4B), further confirming the cardiac developmental defect in *tet2/3*^{DM} larvae. Gene pathway analysis also categorized pathways that were highly downregulated in *tet2/3*^{DM} hearts, including tumor necrosis factor alpha (TNF-α), TGF-β, Notch, and Wnt/beta-catenin signaling pathways (Figure 3F), which highly overlapped with hyper-DMR-related pathways. Taken together, these data link Tet-dependent demethylation with the proper activation of genes critical for cardiac development.

AVC Development Is Disrupted in *tet2/3*^{DM} Larvae Temporally Associated with PE Migration Defect

Both methylomic and transcriptomic analysis identified several pathways that were highly deregulated in 48 hpf *tet2/3*^{DM} hearts, including the Wnt/beta-catenin and TGF-β signaling pathways. Previous studies suggested tight regulation of the Wnt and TGF-β pathways is required for atrioventricular canal (AVC) development at this developmental stage (Azhar et al., 2003; Piven and Winata, 2017). Gene set enrichment analysis from RNA sequencing also showed disruption of epithelial-to-mesenchymal

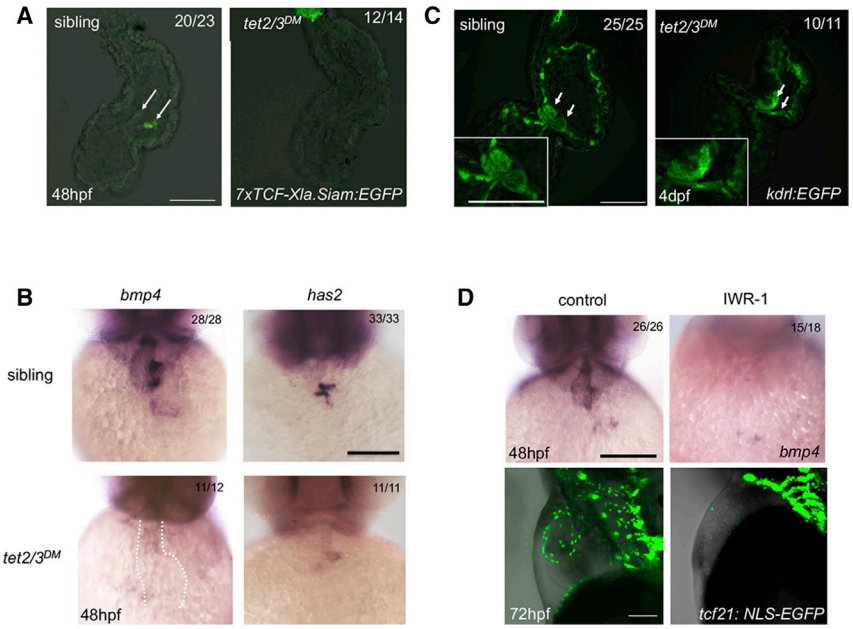

Figure 4. AVC Development Shows Disruption in *tet2/3*^{DM} Larvae

(A) GFP-labeled AVC endocardium represents Wnt activity in sibling heart, but not *tet2/3*^{DM} heart. Hearts were dissected from 48-hpf larvae carrying the Tg(*7xTCF-Xla.Siam:GFP*) transgene. White arrows indicate AVC endocardial cells with Wnt activity.

(B) WISH for AVC markers *bmp4* and *has2* at 48 hpf.

(C) GFP-labeled endocardium represents AV valve formation in 4-dpf sibling, but not *tet2/3*^{DM} larvae carrying the Tg(*kdrl:EGFP*) transgene. White arrows indicate the AV valve. Bottom left images show higher magnification views of AV valve regions.

(D) WISH for AVC marker *bmp4* in 48 hpf and confocal imaging for GFP-labeled PE and epicardium in 72-hpf control and IWR-1-treated larvae. Scale bars: 50 μm.

transition (EMT), extracellular matrix (ECM) organization, and collagen formation in *tet2/3*^{DM} hearts (Figure S4C), all of which are critical processes during AVC development (Moro et al., 2012; Todorovic et al., 2011; Wang et al., 2013). Proper patterning of the AVC is critical for several diverse processes within the developing heart, including cushion and AV valve formation and delay of the electrical impulse between the atria and ventricles (Peal et al., 2011; Wang et al., 2013). The AVC is also the first location where PE cells attach to the heart (Figure 1B), implying its potential function coordinating PE migration. Therefore, we evaluated AVC development in *tet2/3*^{DM} larvae.

During AVC development, endocardial-based Notch-Wnt signaling induces a myocardial Bmp-Tbx pathway, which then activates the expression of downstream ECM-related genes, such as *has2*, to initiate EMT as the first step toward heart valve formation (Shirai et al., 2009; Wang et al., 2013). Using transgenic biosensor reporter strains, we evaluated Notch and Wnt activity in *tet2/3*^{DM} larvae and observed comparable Notch activity in both sibling and *tet2/3*^{DM} endocardium (Figure S4D). We also observed specific Wnt activity in the AVC endocardium in 2 dpf sibling hearts, which is in agreement with previous work (Moro et al., 2012; Wang et al., 2013). However, this Wnt activity signal was strikingly lost in *tet2/3*^{DM} hearts (Figure 4A). By WISH, transcript levels of Wnt downstream genes, including *bmp4*, *tbx2b*, and *has2* (Ahuja et al., 2016; Camenisch et al., 2002; Singh et al., 2012; Verhoeven et al., 2011), were also reduced in the hearts of *tet2/3*^{DM} larvae (Figures 4B and S4E), suggesting a quite early EMT defect in *tet2/3*^{DM} larvae. As a result, the AV valve is absent in 4 dpf *tet2/3*^{DM} larvae (Figure 4C). Moreover, conditional inhibition of the Wnt pathway using a small-molecule compound inhibitor of Wnt response-1 (IWR-1) led to AVC disruption and a PE morphogenesis defect, which phenocopied *tet2/3*^{DM} larvae (Figure 4D), also suggesting a close association of proper AVC patterning and epicardial development.

Hypermethylation and Deregulation of *inhbaa* and *sox9b* Are Associated with AVC Development and PE Migration Defects in *tet2/3*^{DM} Larvae

In order to identify candidate genes targeted by Tet2/3 to regulate AVC development, we filtered data from RNA-seq, 5hMe-BIC-seq, and ERRBS to identify genomic regions associated with genes that are hydroxymethylated in wild-type hearts but hypermethylated, and significantly downregulated, in *tet2/3*^{DM} hearts (Table S1). This identified potential Tet target genes *inhbaa* and *sox9b*, both of which are associated in the literature with regulating AVC development. *Inhbaa* is the monomeric subunit of activin A, a secreted ligand that signals through a serine-threonine kinase complex consisting of type I receptor ActBIB (Alk4) and type II receptor ActRIIA or ActRIIB (DiMuccio et al., 2005; Jaźwińska et al., 2007; Shi and Massagué, 2003; Sun et al., 2006). In murine studies, transcripts for *Inhba* and its receptors were detected in AVC endocardium at embryonic day 9.5 (E9.5) and E10.5, induced by the Notch pathway leading to activation of the nitric oxide (NO) pathway to promote EMT (Chang et al., 2011). After EMT occurs in the AVC endocardium, mesenchymal cells invade and populate ECM to separate the endocardium and myocardium; these progenitors undergo further proliferation to eventually form heart valves (Person et al., 2005; de Vlaming et al., 2012). In mice, *Sox9* is a BMP target required for mesenchymal cell expansion and ECM organization (Garside et al., 2015; Lincoln et al., 2007). In zebrafish studies, *sox9b* was detected in myocardium and required for epicardium as well as valve formation (Hofsteen et al., 2013; Plavicki et al., 2014a).

In *tet2/3*^{DM} larval hearts, both WISH and qPCR showed a clear reduction of *inhbaa* transcripts, which can be rescued by injection of human *TET2* mRNA (Figures 5A and S5A). Because of widespread expression outside of the heart, this loss of *inhbaa* expression is not seen if whole embryos are analyzed; thus, the TET-dependent regulation is heart specific (Figures S5B and S5C). The ERRBS data, validated by gene-specific bisulfite sequencing, identified a hypermethylated region in the promoter of *inhbaa* in *tet2/3*^{DM} hearts, within a broad peak of 5hmC marks that are present in wild-type hearts (Figure 5B). Notably,

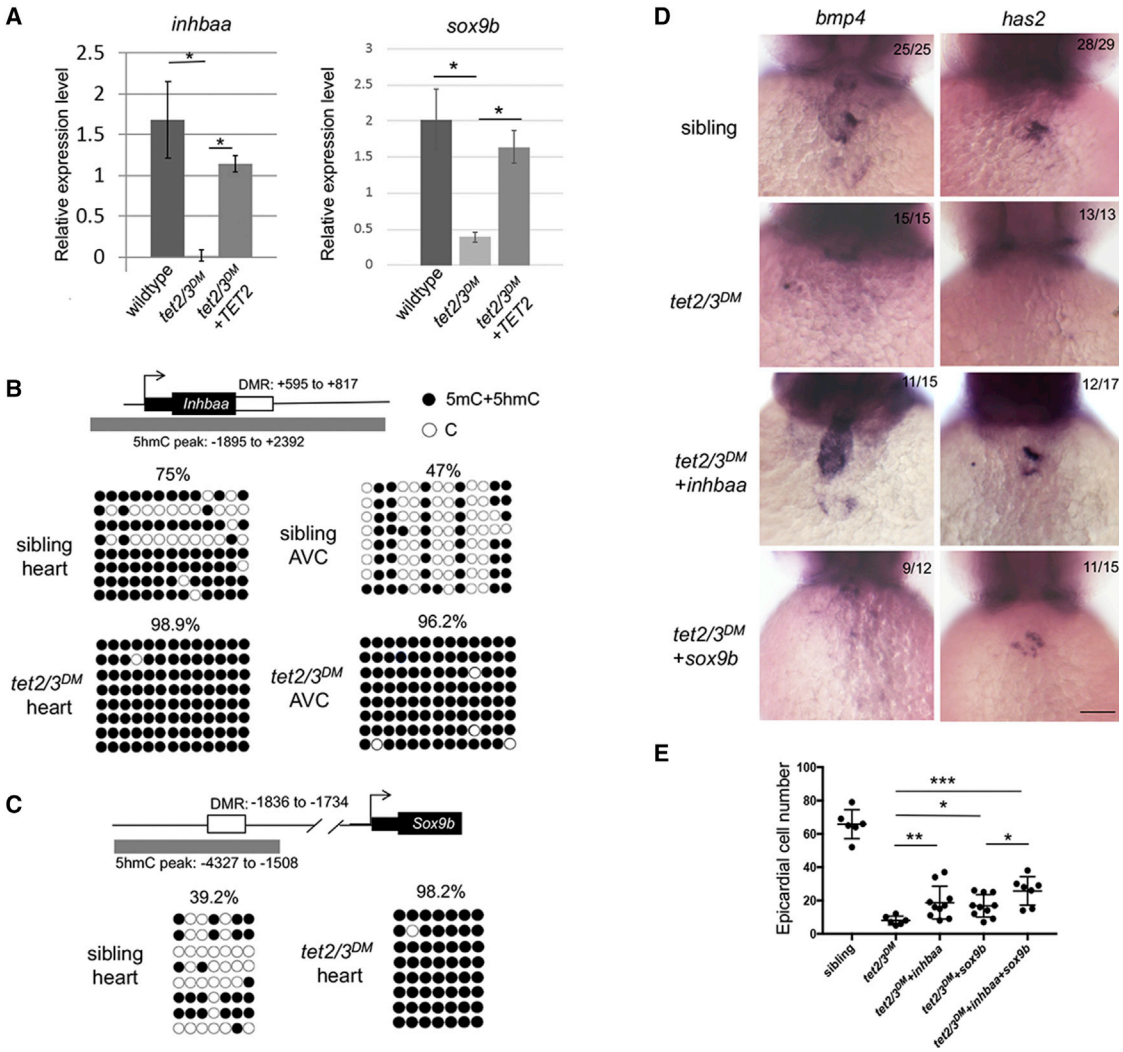

Figure 5. Tet2/3-Dependent Aberrant Promoter Hypermethylation and Deregulation of *inhbaa* and *sox9b* Leads to AVC and PE Migration Defects

(A) RT-PCR analysis of *inhbaa* and *sox9b* transcripts in 48-hpf embryonic heart.

(B) DNA methylation status of *inhbaa* in 48-hpf isolated heart or isolated AVC. Diagram indicates *inhbaa* locus and the associated regulatory regions. Gray box represents 5hmC peak. Black box represents the coding sequence. White box represents hyper-DMR identified by ERRBS. Profiles of 5mC + 5hmC in hyper-DMR region were validated by bisulfite sequencing. n = 4 per condition.

(C) DNA methylation status of *sox9b* in 48 hpf isolated heart. Diagram indicates *sox9b* locus and the associated regulatory regions. Gray box represents 5hmC peak. Black box represents the coding sequence. White box represents hyper-DMR. Profiles of 5mC + 5hmC in hyper-DMR region were validated by bisulfite sequencing. n = 4 per condition.

(D) WISH for AVC markers *bmp4* and *has2* at 48-hpf sibling, *tet2/3*^{DM}, and *tet2/3*^{DM} injected with *inhbaa* mRNA or *sox9b* mRNA larvae. Scale bar: 50 μm.

(E) Number of epicardial cells on the heart of 4-dpf sibling, *tet2/3*^{DM}, and *tet2/3*^{DM} injected with *inhbaa* mRNA, *sox9b* mRNA, or *sox9b* combined with *inhbaa* mRNA larvae carrying the Tg(*tcf21:NLS-EGFP*) transgene. Data are presented as the mean ± SD. The significance is indicated as *p < 0.05; **p < 0.01; ***p < 0.001; ns indicates not significant.

compared with whole heart, the levels of methylation as measured by bisulfite sequencing is further reduced in samples derived from dissected AVC regions, yet this region remains highly methylated in similarly dissected samples derived from *tet2/3*^{DM} hearts (Figure 5B). This AVC-specific methylation pattern is consistent with AVC-enriched transcript expression, suggesting that Tet-dependent DNA demethylation is restricted for this gene largely to AVC endocardium. Similarly, *sox9b* transcripts were also strikingly reduced in the heart, associated with promoter hypermethylation (Figures 5A and 5C), features that were not noted using whole-embryo samples, again indicating cardiac specificity (Figures S5B and S5C). Expression levels for *sox9b* could also be rescued by injection of human *TET2* mRNA (Figure 5A).

To confirm that deregulation of *inhbaa* impacts AVC development as well as PE migration, the small molecule SB431542 was

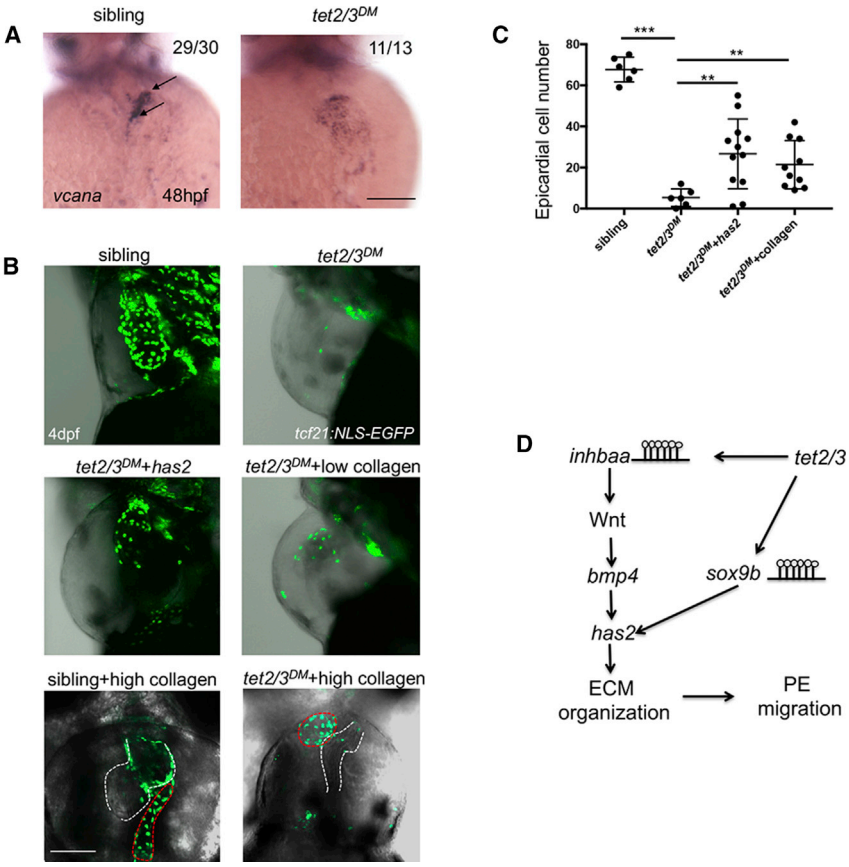

Figure 6. Tet2/3 Regulate PE Migration through Extracellular Matrix Organization

(A) WISH for ECM constituent gene *vcana* at 48 hpf. Black arrows indicate AVC-specific expression of *vcana* in sibling, but not *tet2/3*^{DM} heart.

(B) GFP-labeled PE and epicardium in 4-dpf larvae carrying the Tg(*tcf21:NLS-EGFP*) transgene. Sibling, *tet2/3*^{DM}, and *tet2/3*^{DM} injected with *has2* mRNA and *tet2/3*^{DM} injected with low concentration (0.5 mg/mL) collagen larvae were shown in lateral views. Sibling and *tet2/3*^{DM} injected with high concentration (8 mg/mL) collagen larvae were shown in ventral views to represent collagen aggregate and heart clearly. The heart is outlined with white dashed line. The collagen aggregate is outlined with red dashed line.

(C) Number of epicardial cells on the heart of 4-dpf sibling, *tet2/3*^{DM}, and *tet2/3*^{DM} injected with *sox9b* mRNA or *tet2/3*^{DM} injected with low concentration (0.5 mg/mL) collagen larvae carrying the Tg(*tcf21:NLS-EGFP*) transgene. Numbers data are presented as the mean ± SD derived from 3 independent biological replicates.

(D) Working model shows Tet2/3-dependent demethylation regulates the expression of *inhbaa* and *sox9b*, which subsequently regulate AVC ECM organization and PE migration.

Scale bars: 50 μm. The significance is indicated as *p < 0.05; **p < 0.01; ***p < 0.001.

used to block receptor function, or alternatively, 1-(2-[trifluoromethyl]phenyl)imidazole (TRIM) was used to block the downstream nitric oxide synthase (NOS) inducer. Both treatments caused AVC defects (Figures S6A–S6D) as well as a PE migration defect (Figure S6G). Injection of *inhbaa* mRNA rescued expression of AVC-restricted markers *has2* and *bmp4* (Figure 5D) and partially restored PE migration (Figure 5E). Moreover, TRIM treatment also inhibited Wnt activity in AVC endocardium (Figures S6E and S6F), suggesting that *inhbaa* and NOS function upstream of the Wnt pathway during AVC development. Considering that *Inhba* is regulated by the Notch pathway and our analysis showed no defect for Notch signaling in endocardium of *tet2/3*^{DM} larvae, the data implicate *inhbaa* as a mediator between Notch and Wnt pathways, which is critical for EMT during AVC development. The role of *sox9b* was next tested. Consistent with previous *sox9b* knockdown studies (Hofsteen et al., 2013; Lincoln et al., 2007), epicardial morphogenesis was inhibited in *sox9b* morphant larvae (Figure S6G). Injection of *sox9b* mRNA was sufficient to rescue *has2* but failed to rescue *bmp4* (Figure 5D), indicating that *sox9b* functions downstream of *bmp4* but upstream of *has2*. *Sox9b* mRNA injection also partially restored epicardium in *tet2/3*^{DM} larvae (Figure 5E). Notably, the extent of epicardial rescue in *tet2/3*^{DM} larvae was modestly enhanced with combined injection of *inhbaa* and *sox9b* mRNA (Figure 5E), suggesting that Tet2/3 regulates targets that cooperate to facilitate PE recruitment and epicardial development.

Tet2/3-Dependent AVC ECM Organization Is Critical for PE Attachment to the Heart

In *tet2/3*^{DM} larvae, both *inhbaa* and *sox9b* mRNA rescued expression of the ECM-related gene *has2*, which encodes the enzyme required to synthesize ECM constituent hyaluronic acid. Production of hyaluronan is important for the induction of epicardial cell differentiation and invasion *in vitro* (Craig et al., 2010). Studies in chick embryos also demonstrated that an ECM bridge guides PE cell migration to the myocardium (Nahirney et al., 2003), and we observed features consistent with this process in wild-type zebrafish larvae, lacking in *tet2/3*^{DM} larvae (Figure 1B). These data suggest ECM may play important functions during PE cell migration. Another key AVC-associated ECM constituent protein gene, *vcana* (Hatano et al., 2012), was also strikingly deregulated in *tet2/3*^{DM} larvae (Figure 6A), consistent with RNA sequencing data showing defects of ECM organization and collagen formation in *tet2/3*^{DM} hearts (Figure S4C).

To test directly whether loss of ECM components could account for the PE migration defects observed in *tet2/3*^{DM} larvae, *has2* mRNA was reintroduced into *tet2/3*^{DM} larvae. Injection of *has2* mRNA into *tet2/3*^{DM} embryos increased significantly the number of epicardial cells that migrate onto the heart of tet2/3^{DM} larvae (Figures 6B and 6C). Although *has2* transcript levels were strikingly decreased in *tet2/3*^{DM} hearts, and there were robust 5hmC peaks in the gene body as well as promoter of the *has2* gene in wild-type hearts, we observed no difference in methylation status at these regions comparing genomic DNA isolated from *tet2/3*^{DM} and wild-type hearts (Figure S7). These observations indicate that *has2* is regulated indirectly by

Tet2/3 through *inhbaa* and *sox9b* as a downstream component of Tet-dependent PE morphogenesis.

Finally, we tested directly whether the ECM defect during AVC development is responsible for the PE migration defect by injecting the ECM protein collagen into the pericardial region of *tet2/3*^{DM} larvae at 2 dpf. Strikingly, when *tet2/3*^{DM} larvae were injected with 20 nL of a 0.5 mg/mL collagen solution, PE cells migrated onto the heart tube (Figures 6B and 6C), strongly supporting a non-cell-autonomous effect, specifically through TET-dependent ECM organization at the AVC. Siblings were not affected by this treatment. When a high concentration (8 mg/mL) of collagen solution was injected to the pericardial region, collagen aggregates were formed. Under these conditions, in sibling larvae, the PE cells migrated to the heart as well as attached to the collagen aggregate. In *tet2/3*^{DM} larvae, PE cells were attracted to migrate to the collagen aggregate at the expense of attaching to the heart tube (Figure 6B). Taken together, these results uncover a requirement for Tet2/3 in AVC and epicardial development and identify *inhbaa* and *sox9b* as likely direct targets of Tet2/3 regulation during AVC-associated ECM organization, which then facilitates PE recruitment and attachment to the heart (Figure 6D).

DISCUSSION

During cardiogenesis, epigenetic mechanisms, including DNA methylation and demethylation, histone modification, and long-range chromatin organization, undergo dynamic changes to orchestrate lineage- and temporal-specific changes in gene expression (Backs and Olson, 2006; Hang et al., 2010; Kou et al., 2010; Vallaster et al., 2012), and epigenetic regulatory defects contribute to progression of cardiac diseases (Mano, 2008). However, specific functions and requirements for TET enzymes to regulate DNA demethylation in this context were not known. We found a primary defect in *tet2/3*^{DM} embryos for the attachment to the heart, and subsequent migration to cover the heart, of epicardial progenitors, through defects in PE cell-extrinsic signaling pathways. The results are consistent with recent reports showing cell-non-autonomous functions for Tet enzymes in zebrafish retinal cell differentiation, mouse gastrulation, and for defining the relative balance of neuroectoderm and mesoderm derivatives (Dai et al., 2016; Li et al., 2016; Seritrakul and Gross, 2017). These studies suggest a general function for Tet enzymes during embryonic development to regulate important cell-extrinsic singling pathways and coordinate cell interactions during organ development.

We found that failed recruitment of PE cells to the heart is associated with defective AVC development. Previous loss-of-function studies identified several pathways in the heart, including BMP signaling emanating from the AVC myocardium, that are necessary for recruitment of PE cells (Hatcher et al., 2004; Ishii et al., 2010; Liu and Stainier, 2010; Yang et al., 1995). In our zebrafish model, Tet-dependent expression of activin-A is required to activate a downstream *bmp4* pathway to coordinate the attachment of PE cells to an AVC-associated region of the heart. We also identified *sox9b*, a transcription factor regulating valve precursor cell proliferation and differentiation, as another Tet target gene. Both genes affect ECM scaffold formation. Injection of *has2* mRNA at the one-cell stage or direct injection of collagen into the pericardial region at 2 dpf can efficiently rescue epicardial cell migration onto the heart in *tet2/3*^{DM} larvae. Collagen injection experiments directly demonstrated the important function of ECM organization during PE recruitment to the heart. During cardiac development, ECM provides a bridge linking the AV canal and pericardial wall to help guide PE cell migration to the myocardium. Our data therefore indicate that AVC-specific, ECM-related genes, such as *has2* and *vcana*, are not only critical for AV valve formation within the AV cushions but also appear required for ECM bridge generation in the pericardial cavity.

Because similar numbers of PE cells can be detected in the *tet2/3*^{DM} larvae, and PE cells undergo little if any detectable proliferation at 48 or 72 hpf, Tet2/3 appears to be dispensable for early PE specification and proliferation. However, other cell-autonomous requirements in epicardial cells after they migrate to the heart cannot be ruled out. Because Tet2/3 function is required for EMT during cardiac AVC development and also for endothelial-to-hematopoietic transition (EHT) during hematopoietic stem cell emergence (Li et al., 2015), we speculate that Tet activity becomes progressively more important as specified PE cells become further differentiated and normally undergo EMT (Kalluri and Weinberg, 2009; Kovacic et al., 2012; Krainock et al., 2016). This may represent a common functional requirement for Tet activities in epithelial cells undergoing mesenchymal-like transitions and is likely relevant to the impact of deregulated Tet activity in cancer. Further studies using conditional epicardial lineage-specific knockout of *tet2/3* are needed to clarify the function of Tet during later stages of epicardium-derived cell development.

Consistent with recent studies that identified distal regulatory elements as targets of 5mC remodeling in zebrafish embryogenesis and mouse stem cells (Bogdanović et al., 2016; Hon et al., 2014; Lee et al., 2015), depletion of Tet2/3 causes hypermethylation mainly at normally active enhancers. One study in murine ESCs found that knockdown of Tet1 results in loss of promoter oxidation, and depletion of Tet2 causes loss of 5hmC at gene bodies (Huang et al., 2014). We cannot rule out the possibility that biased enhancer hypermethylation is due to Tet1 activity in *tet2/3*^{DM} larvae. However, in contrast to mouse stem cells, Tet1 expression is low during zebrafish embryogenesis (Ge et al., 2014) and hyper-DMRs are still enriched at enhancers in *tet1/2/3* knockdown larvae (Bogdanović et al., 2016). These data suggest that Tet1 plays a marginal role during zebrafish development. In promoters, CpG islands may be protected against ectopic DNA methylation by additional mechanisms, including exclusion of *de novo* DNMTs and polycomb-associated proteins (Boulard et al., 2015; Noh et al., 2015; Ooi et al., 2007; Rasmussen and Helin, 2016). In contrast, distal regulatory regions, such as enhancers, are more vulnerable to DNMT activity upon loss of Tet activity. Regardless, in the present study, we did identify functional hyper-DMRs in promoter regions (such as for *inhbaa* and *sox9b*). In summary, our study reveals Tet2/3-mediated epigenetic modifications that regulate

cardiogenesis and uncovers molecular pathways in AVC-dependent PE cell recruitment. It also highlights signaling interactions between distinct heart derivatives, including proepicardium, myocardium, and endocardium.

STAR★METHODS

Detailed methods are provided in the online version of this paper and include the following:

- KEY RESOURCES TABLE
- CONTACT FOR REAGENTS AND RESOURCE SHARING
- EXPERIMENTAL MODEL AND SUBJECT DETAILS
  - All procedures were approved by the WCMC IACUC
- METHOD DETAILS
  - RNA Synthesis and Microinjection
  - Whole-mount *in situ* hybridization (WISH)
  - Immunohistochemistry
  - Morpholino and small molecule treatment of embryonic zebrafish
  - Tissue explant culture
  - Collagen injection
  - Image acquisition and analysis
  - RNA isolation and quantitative RT-PCR
  - RNA sequencing
  - ERRBS
  - 5hMe BIC-seq
  - 5mC and 5hmC quantification
- QUANTIFICATION AND STATISTICAL ANALYSIS
- DATA AND SOFTWARE AVAILABILITY

SUPPLEMENTAL INFORMATION

Supplemental Information includes seven figures and two tables and can be found with this article online at https://doi.org/10.1016/j.celrep.2018.12.076.

ACKNOWLEDGMENTS

The authors thank the WCMC Optical Microscopy Core for imaging support; WCMC Epigenomics Core and Genomics Resources Core for performing ERRBS, 5hmC ChIP-seq, and RNA sequencing; Huai-Jen Tsai for providing the Tg(*myl7:EGFP*) transgenic line; Kenneth D. Poss for providing Tg(*tcf21:NLS-EGFP*) and Tg(*tcf21:DsRed2*) transgenic lines; James F. Amatruda for providing the Tg*(7xTCF-Xla.Siam:GFP)*^{ia4} transgenic line; and Jesus Torres Vazquez for providing the Tg*(kdrl:EGFP-NLS)* transgenic line. These studies were supported by a grant from the NHLBI (R35 HL135778 to T.E.) and from the Tri-Institutional Stem Cell Initiative (2014-010 to M.G.G. and T.E.). Y.L. is supported by a Tri-Institutional Starr Stem Cell Scholars Fellowship.

AUTHOR CONTRIBUTIONS

Y.L., M.G.G., and T.E. conceived the study and designed experiments. Y.L. performed most of the experiments. H.P., B.D., and O.E. performed computational and bioinformatics analyses. C.L. provided essential reagents prior to publication. K.M.B. and J.S. performed experiments. Y.L. and T.E. wrote the manuscript. All authors edited and approved of the final draft.

DECLARATION OF INTERESTS

The authors declare no competing interests.

Received: March 27, 2018
Revised: October 30, 2018
Accepted: December 18, 2018
Published: January 15, 2019

REFERENCES

Ahuja, S., Dogra, D., Stainier, D.Y.R., and Reischauer, S. (2016). Id4 functions downstream of Bmp signaling to restrict TCF function in endocardial cells during atrioventricular valve development. Dev. Biol. *412*, 71–82.

Akalin, A., Garrett-Bakelman, F.E., Kormaksson, M., Busuttil, J., Zhang, L., Khrebtukova, I., Milne, T.A., Huang, Y., Biswas, D., Hess, J.L., et al. (2012). Base-pair resolution DNA methylation sequencing reveals profoundly divergent epigenetic landscapes in acute myeloid leukemia. PLoS Genet. *8*, e1002781.

Anelli, V., Villefranc, J.A., Chhangawala, S., Martinez-McFaline, R., Riva, E., Nguyen, A., Verma, A., Bareja, R., Chen, Z., Scognamiglio, T., et al. (2017). Oncogenic BRAF disrupts thyroid morphogenesis and function via twist expression. eLife *6*, e20728.

Azhar, M., Schultz, Jel.J., Grupp, I., Dorn, G.W., 2nd, Meneton, P., Molin, D.G., Gittenberger-de Groot, A.C., and Doetschman, T. (2003). Transforming growth factor beta in cardiovascular development and function. Cytokine Growth Factor Rev. *14*, 391–407.

Backs, J., and Olson, E.N. (2006). Control of cardiac growth by histone acetylation/deacetylation. Circ. Res. *98*, 15–24.

Bogdanovic, O., Fernandez-Miñán, A., Tena, J.J., de la Calle-Mustienes, E., Hidalgo, C., van Kruysbergen, I., van Heeringen, S.J., Veenstra, G.J., and Gómez-Skarmeta, J.L. (2012). Dynamics of enhancer chromatin signatures mark the transition from pluripotency to cell specification during embryogenesis. Genome Res. *22*, 2043–2053.

Bogdanović, O., Smits, A.H., de la Calle Mustienes, E., Tena, J.J., Ford, E., Williams, R., Senanayake, U., Schultz, M.D., Hontelez, S., van Kruijsbergen, I., et al. (2016). Active DNA demethylation at enhancers during the vertebrate phylotypic period. Nat. Genet. *48*, 417–426.

Boulard, M., Edwards, J.R., and Bestor, T.H. (2015). FBXL10 protects polycomb-bound genes from hypermethylation. Nat. Genet. *47*, 479–485.

Burns, C.G., and MacRae, C.A. (2006). Purification of hearts from zebrafish embryos. Biotechniques *40*, 274–278, 276, 278 passim.

Camenisch, T.D., Schroeder, J.A., Bradley, J., Klewer, S.E., and McDonald, J.A. (2002). Heart-valve mesenchyme formation is dependent on hyaluronan-augmented activation of ErbB2-ErbB3 receptors. Nat. Med. *8*, 850–855.

Chang, A.C., Fu, Y., Garside, V.C., Niessen, K., Chang, L., Fuller, M., Setiadi, A., Smrz, J., Kyle, A., Minchinton, A., et al. (2011). Notch initiates the endothelial-to-mesenchymal transition in the atrioventricular canal through autocrine activation of soluble guanylyl cyclase. Dev. Cell *21*, 288–300.

Chen, H.I., Sharma, B., Akerberg, B.N., Numi, H.J., Kivelä, R., Saharinen, P., Aghajanian, H., McKay, A.S., Bogard, P.E., Chang, A.H., et al. (2014). The sinus venosus contributes to coronary vasculature through VEGFC-stimulated angiogenesis. Development *141*, 4500–4512.

Chi, N.C., Shaw, R.M., De Val, S., Kang, G., Jan, L.Y., Black, B.L., and Stainier, D.Y. (2008). Foxn4 directly regulates tbx2b expression and atrioventricular canal formation. Genes Dev. *22*, 734–739.

Craig, E.A., Austin, A.F., Vaillancourt, R.R., Barnett, J.V., and Camenisch, T.D. (2010). TGFβ2-mediated production of hyaluronan is important for the induction of epicardial cell differentiation and invasion. Exp. Cell Res. *316*, 3397–3405.

Dai, H.Q., Wang, B.A., Yang, L., Chen, J.J., Zhu, G.C., Sun, M.L., Ge, H., Wang, R., Chapman, D.L., Tang, F., et al. (2016). TET-mediated DNA demethylation controls gastrulation by regulating Lefty-Nodal signalling. Nature *538*, 528–532.

Dawlaty, M.M., Breiling, A., Le, T., Raddatz, G., Barrasa, M.I., Cheng, A.W., Gao, Q., Powell, B.E., Li, Z., Xu, M., et al. (2013). Combined deficiency of

Tet1 and Tet2 causes epigenetic abnormalities but is compatible with postnatal development. Dev. Cell *24*, 310–323.

Dawlaty, M.M., Breiling, A., Le, T., Barrasa, M.I., Raddatz, G., Gao, Q., Powell, B.E., Cheng, A.W., Faull, K.F., Lyko, F., and Jaenisch, R. (2014). Loss of Tet enzymes compromises proper differentiation of embryonic stem cells. Dev. Cell *29*, 102–111.

de Vlaming, A., Sauls, K., Hajdu, Z., Visconti, R.P., Mehesz, A.N., Levine, R.A., Slaugenhaupt, S.A., Hagège, A., Chester, A.H., Markwald, R.R., and Norris, R.A. (2012). Atrioventricular valve development: new perspectives on an old theme. Differentiation *84*, 103–116.

Dettman, R.W., Denetclaw, W., Jr., Ordahl, C.P., and Bristow, J. (1998). Common epicardial origin of coronary vascular smooth muscle, perivascular fibroblasts, and intermyocardial fibroblasts in the avian heart. Dev. Biol. *193*, 169–181.

DiMuccio, T., Mukai, S.T., Clelland, E., Kohli, G., Cuartero, M., Wu, T., and Peng, C. (2005). Cloning of a second form of activin-betaA cDNA and regulation of activin-betaA subunits and activin type II receptor mRNA expression by gonadotropin in the zebrafish ovary. Gen. Comp. Endocrinol. *143*, 287–299.

Feng, S., Jacobsen, S.E., and Reik, W. (2010). Epigenetic reprogramming in plant and animal development. Science *330*, 622–627.

Garside, V.C., Cullum, R., Alder, O., Lu, D.Y., Vander Werff, R., Bilenky, M., Zhao, Y., Jones, S.J., Marra, M.A., Underhill, T.M., and Hoodless, P.A. (2015). SOX9 modulates the expression of key transcription factors required for heart valve development. Development *142*, 4340–4350.

Ge, L., Zhang, R.P., Wan, F., Guo, D.Y., Wang, P., Xiang, L.X., and Shao, J.Z. (2014). TET2 plays an essential role in erythropoiesis by regulating lineage-specific genes via DNA oxidative demethylation in a zebrafish model. Mol. Cell. Biol. *34*, 989–1002.

Goll, M.G., and Bestor, T.H. (2005). Eukaryotic cytosine methyltransferases. Annu. Rev. Biochem. *74*, 481–514.

Greco, C.M., Kunderfranco, P., Rubino, M., Larcher, V., Carullo, P., Anselmo, A., Kurz, K., Carell, T., Angius, A., Latronico, M.V., et al. (2016). DNA hydroxymethylation controls cardiomyocyte gene expression in development and hypertrophy. Nat. Commun. *7*, 12418.

Hang, C.T., Yang, J., Han, P., Cheng, H.L., Shang, C., Ashley, E., Zhou, B., and Chang, C.P. (2010). Chromatin regulation by Brg1 underlies heart muscle development and disease. Nature *466*, 62–67.

Hatano, S., Kimata, K., Hiraiwa, N., Kusakabe, M., Isogai, Z., Adachi, E., Shinomura, T., and Watanabe, H. (2012). Versican/PG-M is essential for ventricular septal formation subsequent to cardiac atrioventricular cushion development. Glycobiology *22*, 1268–1277.

Hatcher, C.J., Diman, N.Y., Kim, M.S., Pennisi, D., Song, Y., Goldstein, M.M., Mikawa, T., and Basson, C.T. (2004). A role for Tbx5 in proepicardial cell migration during cardiogenesis. Physiol. Genomics *18*, 129–140.

He, Y.F., Li, B.Z., Li, Z., Liu, P., Wang, Y., Tang, Q., Ding, J., Jia, Y., Chen, Z., Li, L., et al. (2011). Tet-mediated formation of 5-carboxylcytosine and its excision by TDG in mammalian DNA. Science *333*, 1303–1307.

Heicklen-Klein, A., and Evans, T. (2004). T-box binding sites are required for activity of a cardiac GATA-4 enhancer. Dev. Biol. *267*, 490–504.

Hofsteen, P., Plavicki, J., Johnson, S.D., Peterson, R.E., and Heideman, W. (2013). Sox9b is required for epicardium formation and plays a role in TCDD-induced heart malformation in zebrafish. Mol. Pharmacol. *84*, 353–360.

Holtzinger, A., Rosenfeld, G.E., and Evans, T. (2010). Gata4 directs development of cardiac-inducing endoderm from ES cells. Dev. Biol. *337*, 63–73.

Hon, G.C., Song, C.X., Du, T., Jin, F., Selvaraj, S., Lee, A.Y., Yen, C.A., Ye, Z., Mao, S.Q., Wang, B.A., et al. (2014). 5mC oxidation by Tet2 modulates enhancer activity and timing of transcriptome reprogramming during differentiation. Mol. Cell *56*, 286–297.

Hu, N., Strobl-Mazzulla, P., Sauka-Spengler, T., and Bronner, M.E. (2012). DNA methyltransferase3A as a molecular switch mediating the neural tube-to-neural crest fate transition. Genes Dev. *26*, 2380–2385.

Huang, C.J., Tu, C.T., Hsiao, C.D., Hsieh, F.J., and Tsai, H.J. (2003). Germ-line transmission of a myocardium-specific GFP transgene reveals critical regulatory elements in the cardiac myosin light chain 2 promoter of zebrafish. Dev. Dyn. *228*, 30–40.

Huang, Y., Chavez, L., Chang, X., Wang, X., Pastor, W.A., Kang, J., Zepeda-Martínez, J.A., Pape, U.J., Jacobsen, S.E., Peters, B., and Rao, A. (2014). Distinct roles of the methylcytosine oxidases Tet1 and Tet2 in mouse embryonic stem cells. Proc. Natl. Acad. Sci. USA *111*, 1361–1366.

Ishii, Y., Garriock, R.J., Navetta, A.M., Coughlin, L.E., and Mikawa, T. (2010). BMP signals promote proepicardial protrusion necessary for recruitment of coronary vessel and epicardial progenitors to the heart. Dev. Cell *19*, 307–316.

Jaźwińska, A., Badakov, R., and Keating, M.T. (2007). Activin-betaA signaling is required for zebrafish fin regeneration. Curr. Biol. *17*, 1390–1395.

Jowett, T. (1999). Analysis of protein and gene expression. Methods Cell Biol. *59*, 63–85.

Kalluri, R., and Weinberg, R.A. (2009). The basics of epithelial-mesenchymal transition. J. Clin. Invest. *119*, 1420–1428.

Kikuchi, K., Gupta, V., Wang, J., Holdway, J.E., Wills, A.A., Fang, Y., and Poss, K.D. (2011). tcf21+ epicardial cells adopt non-myocardial fates during zebrafish heart development and regeneration. Development *138*, 2895–2902.

Kimmel, C.B., Ballard, W.W., Kimmel, S.R., Ullmann, B., and Schilling, T.F. (1995). Stages of embryonic development of the zebrafish. Dev. Dyn. *203*, 253–310.

Ko, M., An, J., Pastor, W.A., Koralov, S.B., Rajewsky, K., and Rao, A. (2015). TET proteins and 5-methylcytosine oxidation in hematological cancers. Immunol. Rev. *263*, 6–21.

Kohli, R.M., and Zhang, Y. (2013). TET enzymes, TDG and the dynamics of DNA demethylation. Nature *502*, 472–479.

Kou, C.Y., Lau, S.L., Au, K.W., Leung, P.Y., Chim, S.S., Fung, K.P., Waye, M.M., and Tsui, S.K. (2010). Epigenetic regulation of neonatal cardiomyocytes differentiation. Biochem. Biophys. Res. Commun. *400*, 278–283.

Kovacic, J.C., Mercader, N., Torres, M., Boehm, M., and Fuster, V. (2012). Epithelial-to-mesenchymal and endothelial-to-mesenchymal transition: from cardiovascular development to disease. Circulation *125*, 1795–1808.

Krainock, M., Toubat, O., Danopoulos, S., Beckham, A., Warburton, D., and Kim, R. (2016). Epicardial epithelial-to-mesenchymal transition in heart development and disease. J. Clin. Med. *5*, 27.

Kranzhöfer, D.K., Gilsbach, R., Grüning, B.A., Backofen, R., Nührenberg, T.G., and Hein, L. (2016). 5′-hydroxymethylcytosine precedes loss of CpG methylation in enhancers and genes undergoing activation in cardiomyocyte maturation. PLoS ONE *11*, e0166575.

Lee, H.J., Lowdon, R.F., Maricque, B., Zhang, B., Stevens, M., Li, D., Johnson, S.L., and Wang, T. (2015). Developmental enhancers revealed by extensive DNA methylome maps of zebrafish early embryos. Nat. Commun. *6*, 6315.

Li, H., and Durbin, R. (2009). Fast and accurate short read alignment with Burrows-Wheeler transform. Bioinformatics *25*, 1754–1760.

Li, X., Lan, Y., Xu, J., Zhang, W., and Wen, Z. (2012). SUMO1-activating enzyme subunit 1 is essential for the survival of hematopoietic stem/progenitor cells in zebrafish. Development *139*, 4321–4329.

Li, C., Lan, Y., Schwartz-Orbach, L., Korol, E., Tahiliani, M., Evans, T., and Goll, M.G. (2015). Overlapping requirements for Tet2 and Tet3 in normal development and hematopoietic stem cell emergence. Cell Rep. *12*, 1133–1143.

Li, X., Yue, X., Pastor, W.A., Lin, L., Georges, R., Chavez, L., Evans, S.M., and Rao, A. (2016). Tet proteins influence the balance between neuroectodermal and mesodermal fate choice by inhibiting Wnt signaling. Proc. Natl. Acad. Sci. USA *113*, E8267–E8276.

Lincoln, J., Kist, R., Scherer, G., and Yutzey, K.E. (2007). Sox9 is required for precursor cell expansion and extracellular matrix organization during mouse heart valve development. Dev. Biol. *305*, 120–132.

Lindsey, S.E., Butcher, J.T., and Yalcin, H.C. (2014). Mechanical regulation of cardiac development. Front. Physiol. *5*, 318.

Liu, J., and Stainier, D.Y. (2010). Tbx5 and Bmp signaling are essential for proepicardium specification in zebrafish. Circ. Res. *106*, 1818–1828.

Loscalzo, J., and Handy, D.E. (2014). Epigenetic modifications: basic mechanisms and role in cardiovascular disease (2013 Grover Conference series). Pulm. Circ. *4*, 169–174.

Madzo, J., Liu, H., Rodriguez, A., Vasanthakumar, A., Sundaravel, S., Caces, D.B.D., Looney, T.J., Zhang, L., Lepore, J.B., Macrae, T., et al. (2014). Hydroxymethylation at gene regulatory regions directs stem/early progenitor cell commitment during erythropoiesis. Cell Rep. *6*, 231–244.

Mano, H. (2008). Epigenetic abnormalities in cardiac hypertrophy and heart failure. Environ. Health Prev. Med. *13*, 25–29.

Meilhac, S.M., Esner, M., Kelly, R.G., Nicolas, J.F., and Buckingham, M.E. (2004). The clonal origin of myocardial cells in different regions of the embryonic mouse heart. Dev. Cell *6*, 685–698.

Moro, E., Ozhan-Kizil, G., Mongera, A., Beis, D., Wierzbicki, C., Young, R.M., Bournele, D., Domenichini, A., Valdivia, L.E., Lum, L., et al. (2012). In vivo Wnt signaling tracing through a transgenic biosensor fish reveals novel activity domains. Dev. Biol. *366*, 327–340.

Nahirney, P.C., Mikawa, T., and Fischman, D.A. (2003). Evidence for an extracellular matrix bridge guiding proepicardial cell migration to the myocardium of chick embryos. Dev. Dyn. *227*, 511–523.

Noh, K.-M., Wang, H., Kim, H.R., Wenderski, W., Fang, F., Li, C.H., Dewell, S., Hughes, S.H., Melnick, A.M., Patel, D.J., et al. (2015). Engineering of a histone-recognition domain in Dnmt3a alters the epigenetic landscape and phenotypic features of mouse ESCs. Mol. Cell *59*, 89–103.

Ooi, S.K., Qiu, C., Bernstein, E., Li, K., Jia, D., Yang, Z., Erdjument-Bromage, H., Tempst, P., Lin, S.P., Allis, C.D., et al. (2007). DNMT3L connects unmethylated lysine 4 of histone H3 to de novo methylation of DNA. Nature *448*, 714–717.

Pan, H., Jiang, Y., Boi, M., Tabbò, F., Redmond, D., Nie, K., Ladetto, M., Chiappella, A., Cerchietti, L., Shaknovich, R., et al. (2015). Epigenomic evolution in diffuse large B-cell lymphomas. Nat. Commun. *6*, 6921.

Parsons, M.J., Pisharath, H., Yusuff, S., Moore, J.C., Siekmann, A.F., Lawson, N., and Leach, S.D. (2009). Notch-responsive cells initiate the secondary transition in larval zebrafish pancreas. Mech. Dev. *126*, 898–912.

Pastor, W.A., Aravind, L., and Rao, A. (2013). TETonic shift: biological roles of TET proteins in DNA demethylation and transcription. Nat. Rev. Mol. Cell Biol. *14*, 341–356.

Patra, C., Diehl, F., Ferrazzi, F., van Amerongen, M.J., Novoyatleva, T., Schaefer, L., Mühlfeld, C., Jungblut, B., and Engel, F.B. (2011). Nephronectin regulates atrioventricular canal differentiation via Bmp4-Has2 signaling in zebrafish. Development *138*, 4499–4509.

Peal, D.S., Lynch, S.N., and Milan, D.J. (2011). Patterning and development of the atrioventricular canal in zebrafish. J. Cardiovasc. Transl. Res. *4*, 720–726.

Peralta, M., González-Rosa, J.M., Marques, I.J., and Mercader, N. (2014). The epicardium in the embryonic and adult zebrafish. J. Dev. Biol. *2*, 101–116.

Person, A.D., Klewer, S.E., and Runyan, R.B. (2005). Cell biology of cardiac cushion development. Int. Rev. Cytol. *243*, 287–335.

Piven, O.O., and Winata, C.L. (2017). The canonical way to make a heart: β-catenin and plakoglobin in heart development and remodeling. Exp. Biol. Med. (Maywood) *242*, 1735–1745.

Plavicki, J.S., Baker, T.R., Burns, F.R., Xiong, K.M., Gooding, A.J., Hofsteen, P., Peterson, R.E., and Heideman, W. (2014a). Construction and characterization of a sox9b transgenic reporter line. Int. J. Dev. Biol. *58*, 693–699.

Plavicki, J.S., Hofsteen, P., Yue, M.S., Lanham, K.A., Peterson, R.E., and Heideman, W. (2014b). Multiple modes of proepicardial cell migration require heartbeat. BMC Dev. Biol. *14*, 18.

Poelmann, R.E., Gittenberger-de Groot, A.C., Mentink, M.M., Bökenkamp, R., and Hogers, B. (1993). Development of the cardiac coronary vascular endothelium, studied with antiendothelial antibodies, in chicken-quail chimeras. Circ. Res. *73*, 559–568.

Rasmussen, K.D., and Helin, K. (2016). Role of TET enzymes in DNA methylation, development, and cancer. Genes Dev. *30*, 733–750.

Ratajska, A., Czarnowska, E., and Ciszek, B. (2008). Embryonic development of the proepicardium and coronary vessels. Int. J. Dev. Biol. *52*, 229–236.

Red-Horse, K., Ueno, H., Weissman, I.L., and Krasnow, M.A. (2010). Coronary arteries form by developmental reprogramming of venous cells. Nature *464*, 549–553.

Reiter, J.F., Alexander, J., Rodaway, A., Yelon, D., Patient, R., Holder, N., and Stainier, D.Y. (1999). Gata5 is required for the development of the heart and endoderm in zebrafish. Genes Dev. *13*, 2983–2995.

Robertson, K.D. (2005). DNA methylation and human disease. Nat. Rev. Genet. *6*, 597–610.

Sen, G.L., Reuter, J.A., Webster, D.E., Zhu, L., and Khavari, P.A. (2010). DNMT1 maintains progenitor function in self-renewing somatic tissue. Nature *463*, 563–567.

Seritrakul, P., and Gross, J.M. (2017). Tet-mediated DNA hydroxymethylation regulates retinal neurogenesis by modulating cell-extrinsic signaling pathways. PLoS Genet. *13*, e1006987.

Serluca, F.C. (2008). Development of the proepicardial organ in the zebrafish. Dev. Biol. *315*, 18–27.

Shi, Y., and Massagué, J. (2003). Mechanisms of TGF-β signaling from cell membrane to the nucleus. Cell *113*, 685–700.

Shirai, M., Imanaka-Yoshida, K., Schneider, M.D., Schwartz, R.J., and Morisaki, T. (2009). T-box 2, a mediator of Bmp-Smad signaling, induced hyaluronan synthase 2 and Tgfbeta2 expression and endocardial cushion formation. Proc. Natl. Acad. Sci. USA *106*, 18604–18609.

Singh, R., Hoogaars, W.M., Barnett, P., Grieskamp, T., Rana, M.S., Buermans, H., Farin, H.F., Petry, M., Heallen, T., Martin, J.F., et al. (2012). Tbx2 and Tbx3 induce atrioventricular myocardial development and endocardial cushion formation. Cell. Mol. Life Sci. *69*, 1377–1389.

Snarr, B.S., Kern, C.B., and Wessels, A. (2008). Origin and fate of cardiac mesenchyme. Dev. Dyn. *237*, 2804–2819.

Solary, E., Bernard, O.A., Tefferi, A., Fuks, F., and Vainchenker, W. (2014). The ten-eleven translocation-2 (TET2) gene in hematopoiesis and hematopoietic diseases. Leukemia *28*, 485–496.

Sun, Z., Jin, P., Tian, T., Gu, Y., Chen, Y.G., and Meng, A. (2006). Activation and roles of ALK4/ALK7-mediated maternal TGFbeta signals in zebrafish embryo. Biochem. Biophys. Res. Commun. *345*, 694–703.

Todorovic, V., Finnegan, E., Freyer, L., Zilberberg, L., Ota, M., and Rifkin, D.B. (2011). Long form of latent TGF-β binding protein 1 (Ltbp1L) regulates cardiac valve development. Dev. Dyn. *240*, 176–187.

Turgeon, P.J., Sukumar, A.N., and Marsden, P.A. (2014). Epigenetics of cardiovascular disease - a new "beat" in coronary artery disease. Med. Epigenet. *2*, 37–52.

Vallaster, M., Vallaster, C.D., and Wu, S.M. (2012). Epigenetic mechanisms in cardiac development and disease. Acta Biochim. Biophys. Sin. (Shanghai) *44*, 92–102.

Verhoeven, M.C., Haase, C., Christoffels, V.M., Weidinger, G., and Bakkers, J. (2011). Wnt signaling regulates atrioventricular canal formation upstream of BMP and Tbx2. Birth Defects Res. A Clin. Mol. Teratol. *91*, 435–440.

Verma, N., Pan, H., Doré, L.C., Shukla, A., Li, Q.V., Pelham-Webb, B., Teijeiro, V., González, F., Krivtsov, A., Chang, C.J., et al. (2018). TET proteins safeguard bivalent promoters from de novo methylation in human embryonic stem cells. Nat. Genet. *50*, 83–95.

Wang, Y., Wu, B., Chamberlain, A.A., Lui, W., Koirala, P., Susztak, K., Klein, D., Taylor, V., and Zhou, B. (2013). Endocardial to myocardial notch-wnt-bmp axis regulates early heart valve development. PLoS ONE *8*, e60244.

Wu, H., and Zhang, Y. (2011). Mechanisms and functions of Tet protein-mediated 5-methylcytosine oxidation. Genes Dev. *25*, 2436–2452.

Wu, X., and Zhang, Y. (2017). TET-mediated active DNA demethylation: mechanism, function and beyond. Nat. Rev. Genet. *18*, 517–534.

Yan, Y.L., Willoughby, J., Liu, D., Crump, J.G., Wilson, C., Miller, C.T., Singer, A., Kimmel, C., Westerfield, M., and Postlethwait, J.H. (2005). A pair of Sox: distinct and overlapping functions of zebrafish sox9 co-orthologs in craniofacial and pectoral fin development. Development *132*, 1069–1083.

Yang, J.T., Rayburn, H., and Hynes, R.O. (1995). Cell adhesion events mediated by alpha 4 integrins are essential in placental and cardiac development. Development *121*, 549–560.

Zhang, Y., Liu, T., Meyer, C.A., Eeckhoute, J., Johnson, D.S., Bernstein, B.E., Nusbaum, C., Myers, R.M., Brown, M., Li, W., and Liu, X.S. (2008). Model-based analysis of ChIP-seq (MACS). Genome Biol. *9*, R137.

Zygmunt, T., Gay, C.M., Blondelle, J., Singh, M.K., Flaherty, K.M., Means, P.C., Herwig, L., Krudewig, A., Belting, H.-G., Affolter, M., et al. (2011). Semaphorin-PlexinD1 signaling limits angiogenic potential via the VEGF decoy receptor sFlt1. Dev. Cell *21*, 301–314.

STAR★METHODS

KEY RESOURCES TABLE

REAGENT or RESOURCE	SOURCE	IDENTIFIER
Antibodies		
p-Histone H3 Antibody (Ser 10)	Santa Cruz	Cat# sc-8656-R; RRID: AB_653256
GFP Monoclonal Antibody (3E6)	Invitrogen	Cat# A-11120; RRID: AB_221568
Bacterial and Virus Strains		
One Shot TOP10 Chemically Competent *E. coli*	Invitrogen	Cat# C404006
Chemicals, Peptides, and Recombinant Proteins		
5-Aza-2_-deoxycytidine	Sigma	A3656-5MG
IWR-1	Enzo Life Sciences	BML-WN103-0005
TRIM(1-[2-(Trifluoromethyl)phenyl]imidazole)	Sigma	T7313-100MG
SB431542	Stemgent	04-0010-10
Corning Collagen I	Fisher	354249
Critical Commercial Assays		
mMESSAGE mMACHINE	Invitrogen	AM1340
RNeasy Mini kit	QIAGEN	74106
RNeasy Micro kit	QIAGEN	74004
LightCycler 480 Sybr Green master mix	Roche	04-887-352-001
Ovation RNA-Seq System V2	Nugen	N/A
TruSeq RNA Library Prep Kit v2	Illumina	RS-122-2001
DNeasy Blood & Tissue Kits	QIAGEN	69506
EZ DNA Methylation-Direct kit	Zymo Research	D5021
Deposited Data		
Raw and analyzed data	This paper	GSE121991
Histone datasets	Bogdanovic et al., 2012	GSE32483
Zebrafish GRCz10 reference genome	Genome Reference Consortium	https://www.ncbi.nlm.nih.gov/assembly/GCF_000002035.5/
Zebrafish danRer7 reference genomes	Wellcome Trust Sanger Institute	https://www.ncbi.nlm.nih.gov/assembly/GCF_000002035.4/
Experimental Models: zebrafish Strains		
tet2$^{mk17/mk17}$, *tet3*$^{mk18/mk18}$ double-mutant (*tet2/3*^{DM})	Li et al., 2015	N/A
Tg*(myl7:EGFP)*	Huang et al., 2003	N/A
Tg*(tcf21:NLS-EGFP)*	Kikuchi et al., 2011	N/A
Tg *(tcf21:DsRed2)*	Kikuchi et al., 2011	N/A
Tg*(7xTCF-Xla.Siam:GFP)*^{ia4}	Moro et al., 2012	N/A
Tg*(kdrl:EGFP-NLS)*	Zygmunt et al., 2011	N/A
Tg*(tp1:EGFP)*	Parsons et al., 2009	N/A
Oligonucleotides		
Splice-blocking MO (5′ TGC AGT AAT TTA CCG GAG TGT TCT C 3′) for *sox9b*	Yan et al., 2005	N/A
PCR primer sequences, see Table S1	This paper	N/A
Recombinant DNA		
Plasmid: pEF1/V5-His-hTET2	Li et al., 2015	N/A
Plasmid: pEF1/V5-His-mutant hTET2	Li et al., 2015	N/A
Plasmid: pCS2+-*inhbaa*	This paper	N/A
Plasmid: pCS2+-*sox9b*	This paper	N/A
Plasmid: pCS2+-*has2*	This paper	N/A

(*Continued on next page*)

Continued

REAGENT or RESOURCE	SOURCE	IDENTIFIER
Software and Algorithms		
SPOT advanced imaging software	SPOT Imaging	N/A
Zen software	ZEISS	N/A
macs14 1.4.2	Shirley Liu lab	http://liulab.dfci.harvard.edu/MACS/00README.html
Lasergene	DNASTAR	N/A
Prism 7	Graphpad	N/A

CONTACT FOR REAGENTS AND RESOURCE SHARING

Further information and requests for reagents should be directed to and will be fulfilled by Todd Evans (tre2003@med.cornell.edu).

EXPERIMENTAL MODEL AND SUBJECT DETAILS

All procedures were approved by the WCMC IACUC

Zebrafish: We used 1–4 days post fertilization larval zebrafish for this study, bred on AB background. Embryos were raised at 28.5°C and morphologically staged as described (Kimmel et al., 1995); No statistical methods were used to predetermine sample size, and animal selection was not randomized or blinded.

Previously described zebrafish lines were used as follows:: *tet2*$^{mk17/mk17}$, *tet3*$^{mk18/mk18}$ double mutant (*tet2/3*^{DM}) (Li et al., 2015) for *tet2/3* loss of function studies, Tg*(myl7:EGFP)* (Huang et al., 2003) for myocardium labeling, Tg*(tcf21:NLS-EGFP)* and Tg *(tcf21:DsRed2)(* Kikuchi et al., 2011) for epicardium labeling, Tg*(7xTCF-Xla.Siam:GFP)*^{ia4} (Moro et al., 2012) for Wnt pathway activity labeling, Tg*(kdrl:EGFP-NLS)* (Zygmunt et al., 2011) for endothelium labeling, Tg*(tp1:EGFP)* (Parsons et al., 2009) for Notch pathway activity labeling.

Embryos selected for experiments were typically less than 4dpf, a stage at which sex cannot be readily determined and is unlikely to influence the biological processes under study.

METHOD DETAILS

RNA Synthesis and Microinjection

The human *TET2* vector used for mRNA production has been previously described (Li et al., 2015). Briefly, the human *TET2* ORF corresponding to GenBank: NM_001127208 was amplified from cDNA made from SH-SY5Y neuroblastoma cells. Following sub-cloning, the *TET2* ORF was introduced into the pEF1/V5-His vector (Invitrogen) to allow for *in vitro* transcription. Mutant *TET2* (H1382Y, D1384A) was generated using the QuikChange Lightning Site-Directed Mutagenesis Kit (Agilent). The *inhbaa, sox9b* and *has2* ORF were PCR amplified from a 2 dpf zebrafish embryo cDNA library and cloned into the pCS2+ vector. Sequences of all clones were confirmed by conventional DNA sequencing. PCR primers used are listed in Table S1. Capped RNA was synthesized using mMESSAGE mMACHINE (Invitrogen) with Sp6 polymerase. For each experimental condition, mRNA was injected into at least 100 embryos derived from *tet2*$^{mk17/mk17}$, *tet3*$^{mk18/+}$ intercrosses.

Whole-mount *in situ* hybridization (WISH)

Zebrafish embryos at the desired stages were fixed in 4% paraformaldehyde (PFA). Whole-mount RNA *in situ* hybridization (WISH) was performed using standard methods (Jowett, 1999). For *inhbaa* heart *in situ*, embryonic hearts were micro-dissected at 2 dpf and processed with a standard WISH protocol. For *inhbaa* and *has2* probe generation, the same vectors used for RNA synthesis were linearized by EcoRI (*inhbaa*) or BamHI (*has2*). The riboprobe was synthesized with T7 RNA polymerase. Additional probes were prepared as described previously: *nkx2.5*, *amhc*, *vmhc* (Reiter et al., 1999); *gata4* (Heicklen-Klein and Evans, 2004); *wt1* (Serluca, 2008); *bmp4* and *tbx2b* (Chi et al., 2008); *vcana* (Patra et al., 2011), *sox9b* (Yan et al., 2005).

Immunohistochemistry

Whole-mount immunohistochemistry was performed using standard methods (Li et al., 2012). Anti-pH3 primary antibody (Santa Cruz) was used at 1:3000 dilution. Anti-GFP primary antibody (Invitrogen) was used at 1:1000 dilution. Alexa Fluor 555-conjugated anti-rabbit and Alexa Fluor 488-conjugated anti-mouse secondary antibodies (Invitrogen) were used at 1:2000 dilution.

Morpholino and small molecule treatment of embryonic zebrafish

Splice-blocking MO (5′ TGC AGT AAT TTA CCG GAG TGT TCT C 3′) for *sox9b* was as described (Yan et al., 2005) and injected into one cell stage embryos. For chemical treatment, wild-type or *tet2/3*^{DM} embryos were manually dechorionated with forceps at 24 hpf

and exposed to 5-aza (75 μM, Sigma), IWR-1(10 μM, Enzo Life Sciences), TRIM (2 μM, Sigma), or SB431542 (100 μM, Stemgent) from 24 hpf to identical stages for analysis in a solution of E3 medium (5.0 mM NaCl, 0.17 mM KCl, 0.33 mM CaCl, 0.33 mM MgSO4).

Tissue explant culture

Hearts from *myl7:EGFP* and *tcf21:DsRed2* larvae were isolated at 48 hpf and 72 hpf, respectively, as previously described (Burns and MacRae, 2006). Briefly, approximately 100 embryos were anesthetized, washed three times with embryo disruption medium (EDM) [Leibovitz's L-15 Medium (Fisher) containing 10% fetal bovine serum (Sigma), ice-cold at every step] and resuspended in 1.25 mL EDM. The microfuge tube, a 19-gauge needle and a 6-mL syringe were secured to a ring stand. Approximately 1 mL EDM containing embryos was drawn into the needle and syringe and immediately expelled back into the microfuge tube 30 times at a rate of 1 s per syringe motion. Isolated hearts were isolated under a fluorescence microscope. Hearts were mixed in a 1:1 ratio and placed in culture plates coated with low melting agarose. Heart cultures were incubated at 28°C in tissue culture media containing Leibovitz's L-15 (Fisher) with 10% fetal bovine serum (Sigma) and 4x penicillin/streptomycin (Invitrogen). Cultures were monitored daily and media was refreshed every other day. On day 7, heart clusters were removed and imaged by confocal microscopy.

Collagen injection

For low concentration (0.5mg/ml) collagen injection, Corning Collagen I, High Concentration, Rat Tail (Fisher, 8mg/ml) was diluted in tissue culture medium. 20nl of diluted collagen was microinjected into the pericardial region of 2 dpf larvae. For high concentration collagen injection, 10nl of 8mg/ml collagen was directly microinjected into the pericardial region of 2 dpf larvae to generate a collagen aggregate.

Image acquisition and analysis

WISH preparations were mounted in glycerol and imaged using a Nikon SMZ1500 microscope with an Insight Firewire 2 digital camera and SPOT advanced imaging software. Transgenic embryos, embryonic hearts and cultured heart clusters were mounted in low melting agarose and imaged using the Zeiss LSM510 or LSM800 confocal microscope with Zen software. Images were analyzed in ImageJ and Adobe Photoshop. Epicardial cell number was counted manually at 4 dpf using the Zeiss LSM510 confocal microscope. 4% tricaine (Sigma) was added immediately before counting to stop heart beating. At least 10 embryos were counted for each biological replicate.

RNA isolation and quantitative RT-PCR

Whole embryo and dissected heart total RNA was isolated with the RNeasy Mini kit (QIAGEN) or RNeasy Micro kit (QIAGEN). At least 5 fish or 40 dissected hearts were used for each biological replicate. RNA was reverse transcribed with the Superscript III First-Strand Synthesis System (Invitrogen). The qPCR analysis was performed on a LightCycler 480 II (Roche) using LightCycler 480 Sybr Green master mix (Roche). Primer sequences are provided in Table S1. Relative gene expression was determined as described (Holtzinger et al., 2010).

RNA sequencing

For RNA sequencing, whole embryo (n = 3) or dissected heart (n = 2) total RNA from wild-type, sibling or *tet2/3*^{DM} embryos were isolated as described above. For dissected heart, 1 ng total RNA was used to prepare amplified double-stranded cDNA using the Ovation RNA-Seq System V2 (Nugen). Amplified cDNA was purified using a QIAquick PCR purification kit (QIAGEN) and 200 ng of amplified cDNA was fragmented in a final volume of 50 ul using S220 Focused-ultrasonicator (Covaris) to obtain 150 bp DNA fragment size (peak incident power: 175W, duty factor: 10%, cycles per burst: 200, time: 280 s). Fragmented DNA samples and whole embryo RNA samples were used to prepare libraries with the TruSeq RNA Library Prep Kit v2 (Illumina) and submitted to WCMC Genomics Resources Core Facility for sequencing. RNA-seq data were aligned to the GRCz10 reference genome. RNA seq alignment, differential gene expression analysis, orthology to human genes and GSEA were performed as described (Anelli et al., 2017). Differentially expressed genes were defined by log2 fold change greater than 2 or less than −2 and an adjusted p value < 0.05.

ERRBS

For ERRBS, genomic DNA was isolated from wild-type and *tet2/3*^{DM} dissected hearts using DNeasy Blood & Tissue Kits (QIAGEN). At least 40 hearts were collected for each biological group. Genomic DNA was submitted to the Weill Cornell Medical College Epigenomics core for ERRBS. The WCMC Computational Genomics core facility supported alignment and methylation extraction for ERRBS data as described (Akalin et al., 2012). DMRs were defined as regions containing at least five differentially methylated CpGs (DMCs; false discovery rate = 20%; chi-square test) and whole methylation was more than 10%. DMR calling was performed with RRBSeeqer with default parameters (Pan et al., 2015). Peak annotation was performed with R-3.3.2. Histone datasets were obtained from GSE32483 (Bogdanovic et al., 2012).

5hMe BIC-seq

Genomic DNA was isolated from wild-type (n = 2) dissected hearts using DNeasy Blood & Tissue Kits (QIAGEN). At least 40 hearts were collected for each biological group. Genomic DNA was submitted to the Weill Cornell Medical College Epigenomics core for 5hMe-Bead-Integrated Click-seq (5hMe BIC-seq) as described below:

250 ng of genomic DNA were sonicated in a Covaris S220 instrument (Covaris, Woburn, MA) to obtain mean fragment sizes of 250bp (Peak Incident Power 175, Duty Factor 10%, Cycles per Burst 200, 150secs) and DNA was end-repaired and A-tailed using New England Biolabs enzymes (Ipswich, MA). 10ng of this DNA was used as Input control by adding TruSeq barcoded adapters. The rest of the sample was used to selectively label 5-hydroxymethylcytosine with azido-modified-glucose (UDP-6-N3_Glucose, P19-11019, Proactive Molecular Research, Alachua, FL) in the presence of b-glucosyltransferase (New England Biolabs, Ipswich, MA) by a 16 hr incubation at 37C. Biotin was added through Click chemistry with Dibenzocyclooctyne-PEG4-biotin (BP-22295, BroadPharm, San Diego, CA), and the biotinylated-gluco-modified DNA was isolated by affinity capture with streptavidin magnetic beads (Dynabeads ® MyOneStreptavidin, ThermoFisher/LifeTechnologies, Waltham, MA). After ligation of TruSeq barcode adapters the 5hmC-enriched sample was PCR amplified using 12 cycles with Turbo Pfu Cx Polymerase (Agilent, Santa Clara, CA). To control the labeling and enrichment of 5hmC-containing DNA, a parallel reaction containing sheared *E. coli* DNA spiked in with the 5-hydroxymethylcytosine APC-spike control (cat # 55008) obtained from Active Motif (Carlsbad, CA) was performed. Input and 5hmC-enriched libraries were clustered on a paired end read flow cell and sequenced for 50 cycles on an Illumina HiSeq 2500 to obtain about 30M reads per libraries. Primary processing of sequencing images was done using Illumina Real Time Analysis software (RTA) as suggested by Illumina. CASAVA 1.8.2 software was used to perform image capture, base calling and demultiplexing. Reads passing Illumina's purity filter were adaptor trimmed and aligned to the genome using the BWA aligner.

ChIP-seq data were aligned to the danRer7 reference genomes using bwa-0.7.12 with default parameters by the WCMC Computational Genomics core facility (Li and Durbin, 2009). Peak calling and analysis of read density in peak regions were performed by macs14 1.4.2 with default parameters (Zhang et al., 2008).

5mC and 5hmC quantification

Bisulfite sequencing was performed using the EZ DNA Methylation-Direct kit (Zymo Research). Embryonic hearts at 48 hpf were dissected (n = 4 per condition). Converted DNA was amplified using Taq DNA Polymerase (NEB) and bisulfite-specific primer pairs (listed in Table S1). PCR amplicons were sub-cloned using the TOPO TA Cloning kit (Invitrogen) for sequencing. At least 8 clones were sequenced for each condition. Sequencing traces were analyzed using Lasergene (DNASTAR).

QUANTIFICATION AND STATISTICAL ANALYSIS

The Student unpaired 2-tailed t test was used for statistical analysis. We performed Shapiro-Wilk normality tests and all samples passed the test; therefore, we could justify using parametric tests (t test). Data are presented as mean ± SD derived from at least three independent biological replicates. Statistical analysis was performed using Excel and Prism 7. The significance is indicated as *$p < 0.05$, **$p < 0.01$, ***$p < 0.001$, ns indicates not significant.

DATA AND SOFTWARE AVAILABILITY

The accession number for all the sequencing data reported in this paper is NCBI GEO: GSE121991.

Cell Reports, Volume *26*

Supplemental Information

TETs Regulate Proepicardial Cell Migration through Extracellular Matrix Organization during Zebrafish Cardiogenesis

Yahui Lan, Heng Pan, Cheng Li, Kelly M. Banks, Jessica Sam, Bo Ding, Olivier Elemento, Mary G. Goll, and Todd Evans

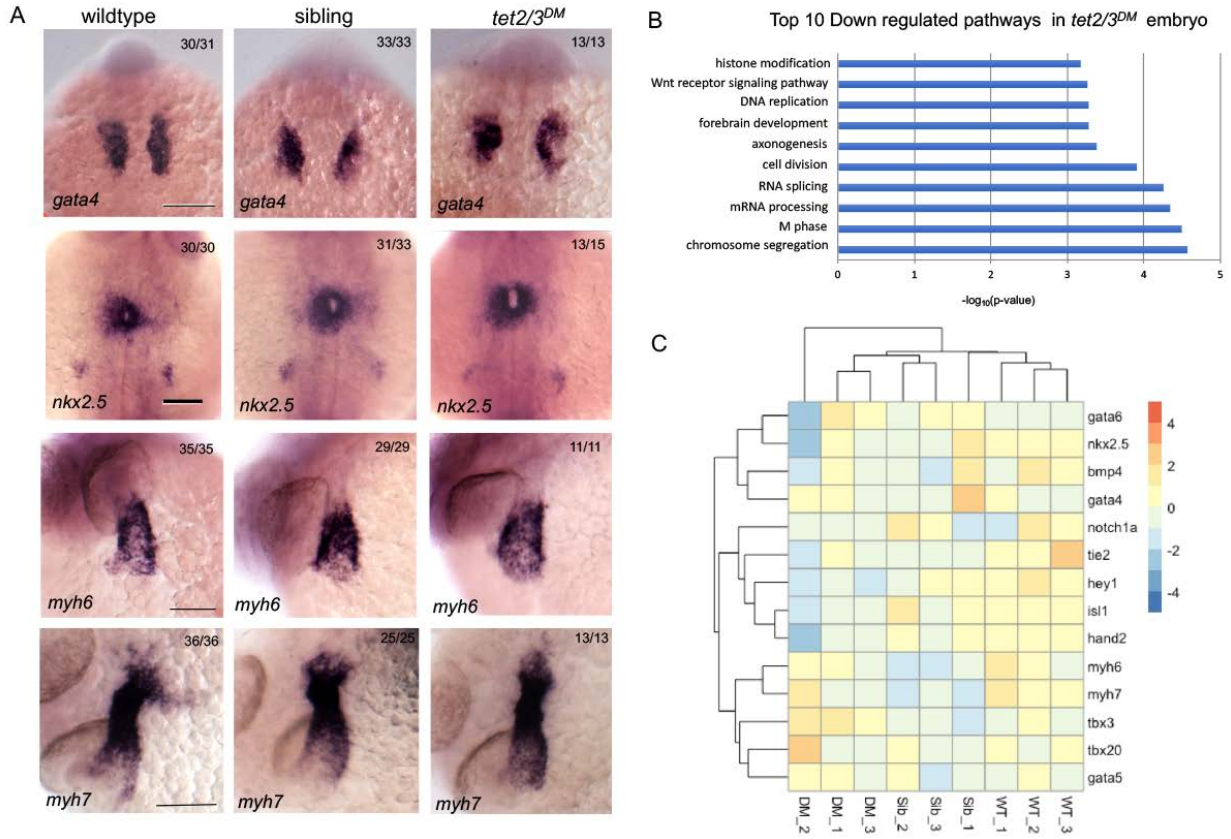

Figure S1: *tet2/3*^{DM} Larvae Show Neuronal but not Cardiac Defects at 28 hpf. Related to Figure 1.

(A) Markers of cardiac progenitors are similarly expressed in wildtype, sibling and *tet2/3*^{DM} larvae. WISH for *gata4* was performed at 18 hpf, *nkx2.5* was performed at 22-hpf, atrial myosin marker *myh6* and myosin marker *myh7* were performed at 28-hpf. Scale bar: 100 μm.
(B) Gene ontology (GO) analysis shows top ten down-regulated biological pathways in 28-hpf *tet2/3*^{DM} larvae by RNA sequencing.
(C) Heatmap of RNA sequencing data illustrating similar transcriptional expression of cardiac genes in *tet2/3*^{DM} (DM) compared with wildtype (WT) or sibling (Sib) larvae.

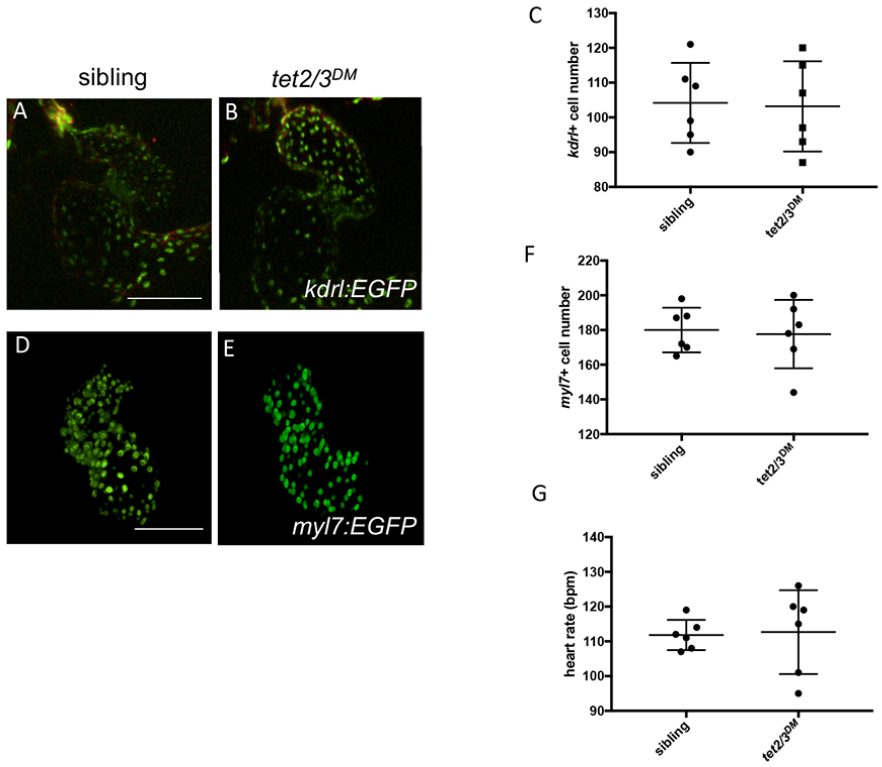

Figure S2: Normal Myocardium and Endocardium in 2-dpf *tet2/3^{DM}* Larvae. Related to Figure 1.
(A and B) GFP labeled endocardium in 2-dpf larvae carrying the Tg(*kdrl:EGFP-NLS)* transgene.
(C) Graph indicates the number of endocardial cells in 48-hpf sibling and *tet2/3^{DM}* larvae. Data are presented as the mean ± SD.
(D and E) GFP labeled myocardium in 2-dpf larvae carrying the Tg(*myl7:EGFP)* transgene.
(F) Graph indicates the number of myocardial cells in 48-hpf sibling and *tet2/3^{DM}* larvae. Data are presented as the mean ± SD.
(G) Graph indicates heart rate in 48-hpf sibling and *tet2/3^{DM}* larvae. Heart rate was measured in beats per minute. Data are presented as the mean ± SD.
Scale bars: 100 μm.

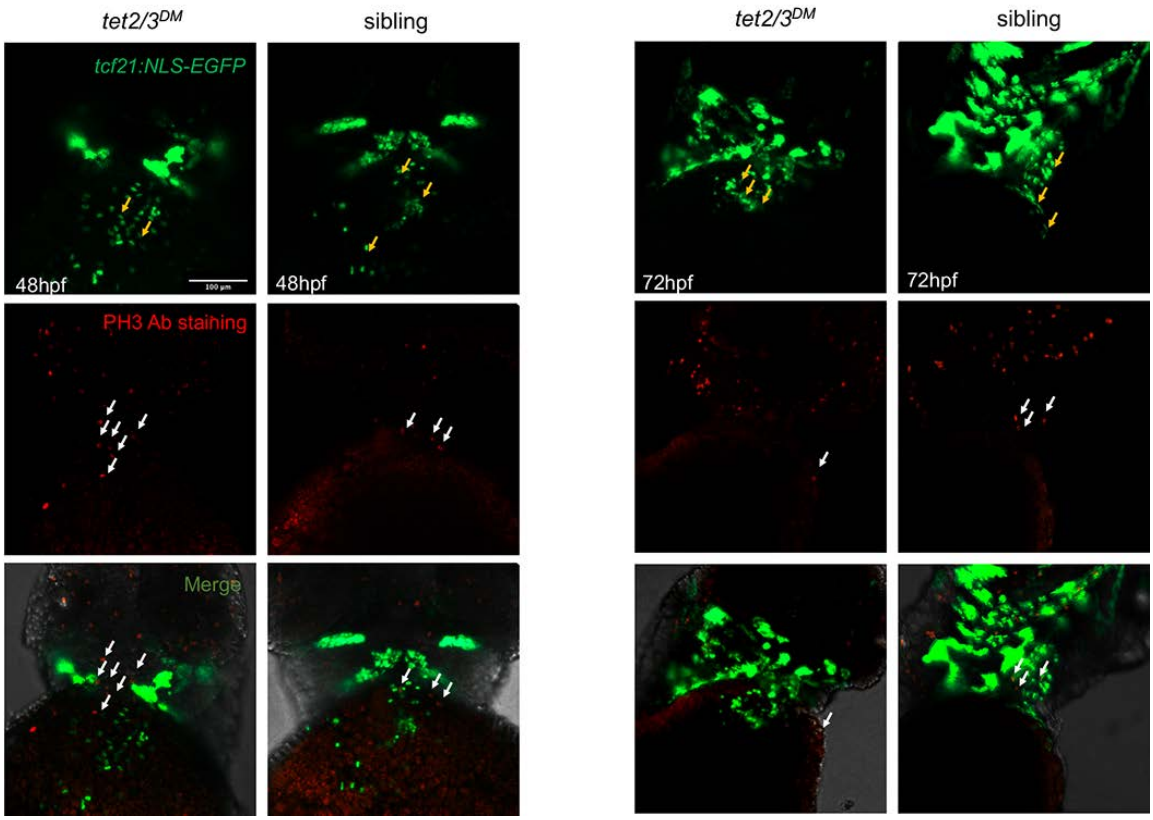

Figure S3: No PE Cell Proliferation at 48 and 72 hpf Sibling and *tet2/3^{DM}* Larvae. Related to Figure 1.
Confocal images showing sibling and *tet2/3^{DM}* larvae carrying the Tg(*tcf21:NLS-EGFP*) transgene stained by anti-GFP antibody (Green) plus anti-pH3 antibody (Red). Yellow arrows indicate PE cells. White arrows indicate pH3+ proliferating cells. Co-staining shows essentially no cell proliferation of *tcf21*+ PE cells at 48-hpf or 72-hpf.
Scale bar: 100 μm.

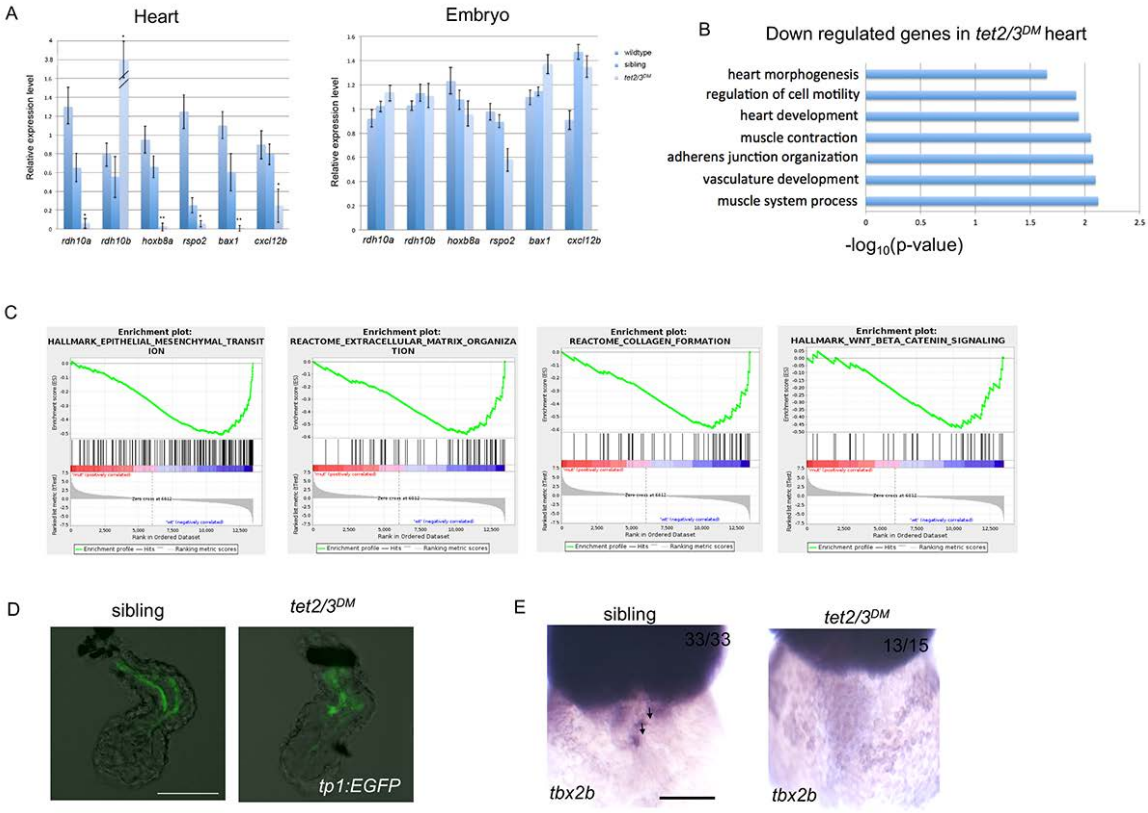

Figure S4: *tet2/3^{DM}* Larvae Show Cardiac AVC Defects at 48-hpf. Related to Figure 3 and Figure 4.
(A) Quantitative RT-PCR validation of top down-regulated genes from RNA sequencing. RT-PCR analysis of *rdh10a, hoxb8a, rspo2, bax1, cxcl12b* transcripts in 2-dpf embryonic heart or whole embryo. Notably, *rdh10b* apparently compensates for the *rdh10a* loss, with 4-fold increase in *tet2/3^{DM}* hearts, which is consistent with RNA sequencing results.
(B) GO analysis shows down-regulated biological pathways in 48 hpf *tet2/3^{DM}* hearts compared to wildtype hearts by RNA sequencing using isolated hearts.
(C) Gene set enrichment analysis shows down-regulated biological pathways in 48-hpf tet2/3DM hearts compared to wildtype hearts by RNA sequencing using isolated hearts.
(D) Normal Notch Activity in tet2/3DM endocardium. GFP-labeled atrial endocardium indicates Notch activity in sibling hearts as well as tet2/3DM hearts. Hearts were dissected from 48 hpf larvae carrying the Tg(*tp1:EGFP*) Notch reporter transgene.
(E) WISH for AVC markers *tbx2b* at 48 hpf. Black arrows indicate AVC specific expression of *tbx2b* in sibling but not *tet2/3^{DM}* heart. Scale bars: 50µm.

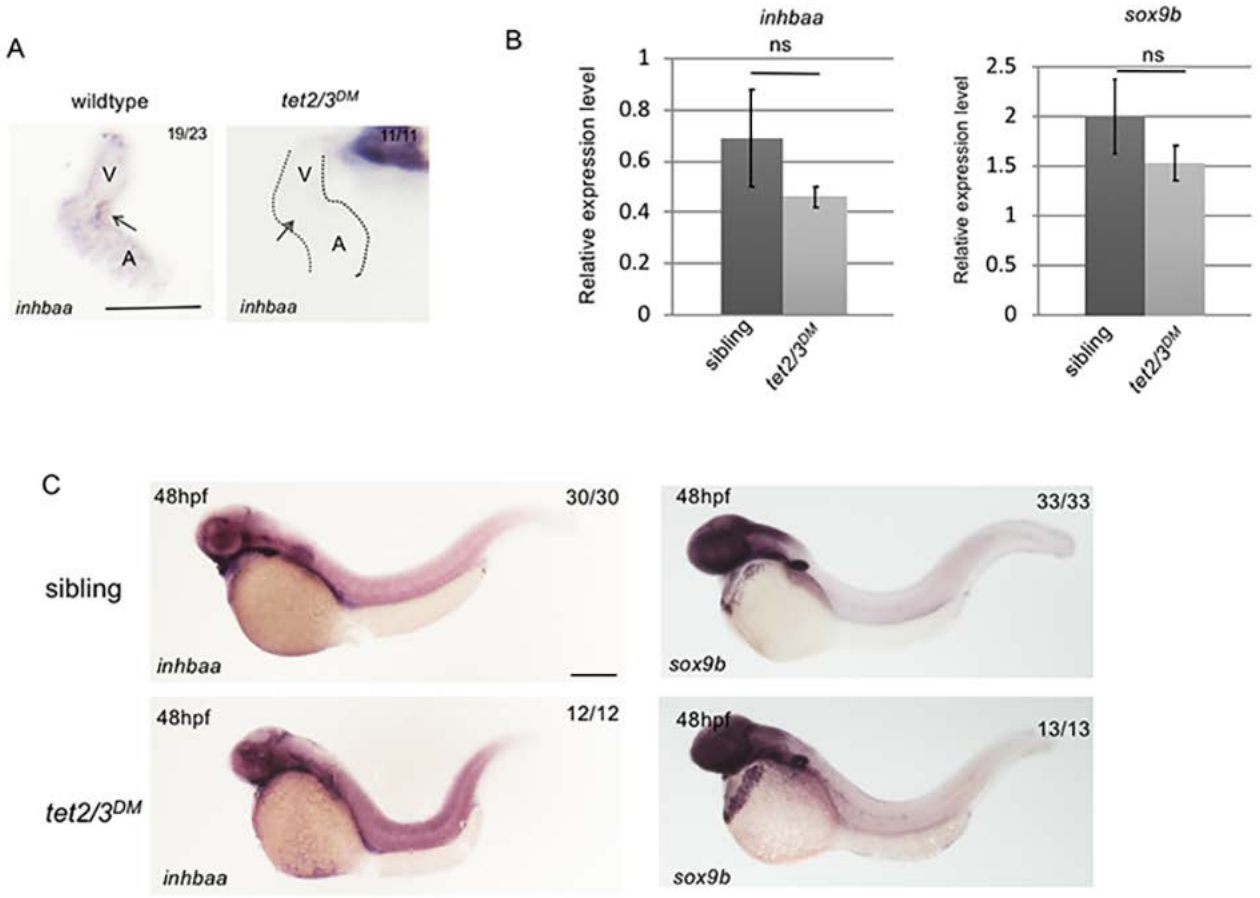

Figure S5: *inhbaa* and *sox9b* Expression Shows Cardiac Specific Defects in *tet2/3*^{DM} Larvae. Related to Figure 5.

(A) WISH for *inhbaa* at 48-hpf isolated hearts. Arrows indicate AVC endocardium with *inhbaa* transcripts. Scale bar: 100 µm.

(B) RT-PCR analysis of *inhbaa* and *sox9b* transcripts in representative 48-hpf embryos.

(C) WISH for *inhbaa* and *sox9b* in representative 48-hpf embryos. Scale bar: 300 µm.

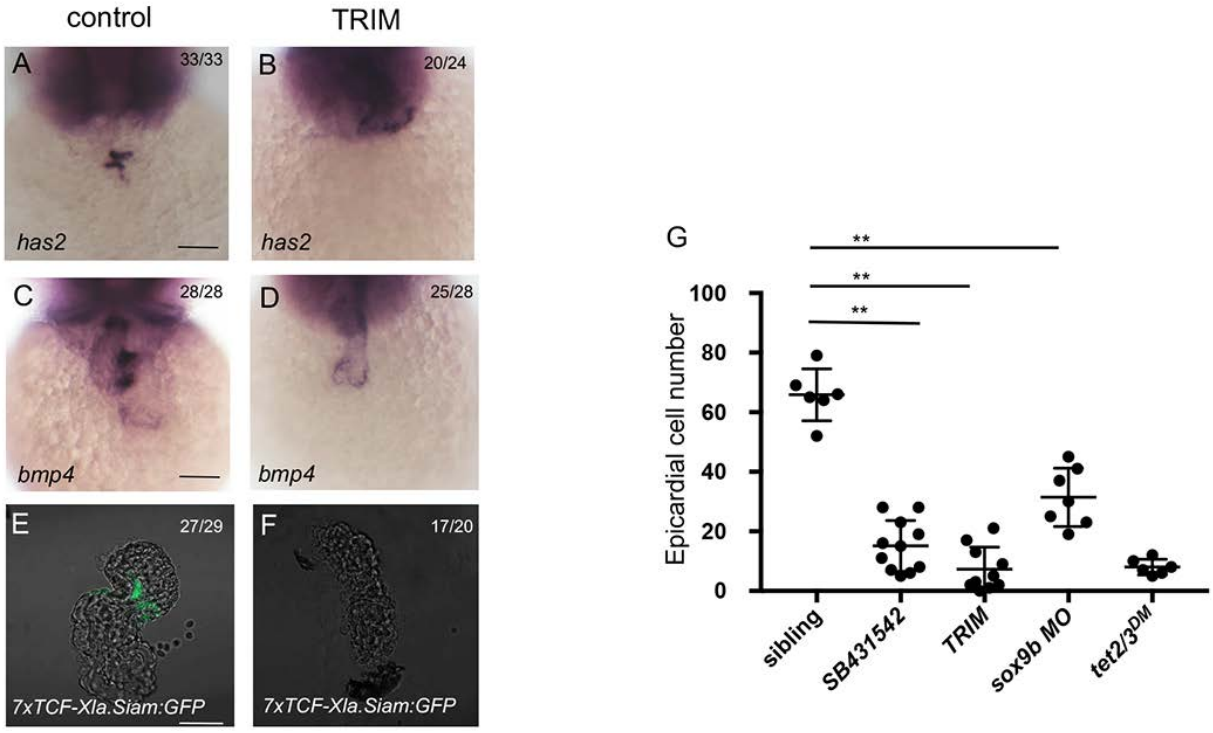

Figure S6: Inhibiting the Activin-A Pathway or *sox9b* Causes AVC Disruption and PE Migration Defect. Related to Figure 5.

(A-D) WISH for AVC markers *has2* and *bmp4* at 48-hpf in wildtype or TRIM treated larvae.

(E-F) GFP-labeled AVC endocardium represents Wnt activity in wildtype but not TRIM treated heart. Hearts were dissected from 48-hpf larvae carrying the Tg(*7xTCF-Xla.Siam:GFP*) transgene.

(G) Number of epicardial cells in the heart of 4-dpf sibling, sibling exposed to SB431542 or TRIM from 24 hpf, *sox9b* morphant and *tet2/3*^{DM} larvae carrying the Tg(*tcf21:NLS-EGFP*) transgene. Data are presented as the mean ± SD. The significance is indicated as **P < 0.01.

Scale bar: 50μm.

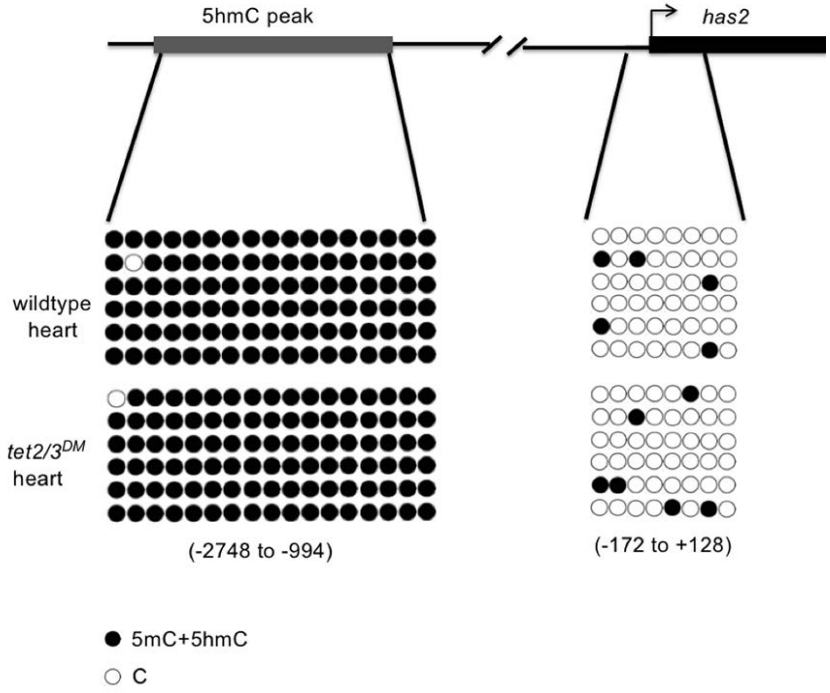

Figure S7. No Hypermethylation at the Promoter of the *has2* Gene in *tet2/3^{DM}* Hearts. Related to Figure 6.

Diagram indicates *has2* locus and the associated regulatory regions. Gray box represents a 5hmC peak. Black box represents the coding sequence. Profiles of 5mC + 5hmC in the putative promoter regions revealed by bisulfite sequencing. Numbers indicate regions analyzed relative to the translation start site.

bis-sequence primer		5'--3'
inhbaa	F	TTTGGGGGGGGGGTTTTTATTG
	R	AATAAAAAAACACATACTTAACATACTAC
sox9b	F	TGTGTTTATTTGTGTTGGTGATGTTGTGG
	R	ACAAAAAACTACAATAACCATACTAAAATCTC
has2-promoter	F1	GTATGTTTGTATTGTGGGGGAAATTTGAGGGTTTGGAG
	R1	TCATTATTTCATTCATTTTCTTTTCAACTTAATCCC
	F2	AAAAGATTGTTGAGGTGTTGAAGG
	R2	CAAAATCAATTACACATAACCTCTCAATAATAC
has2-exon1	F	ATTTGAAGGGGTAGTATTTTTTTTTTTTAGATGTTG
	R	CATTCAAATTTTTTTTTTCCCCAAAC

qRT-PCR primer		5'---3'
inhbaa	F	GCACATTCAGAAGCCGACTGCC
	R	TAAAGTCCGTCTGCCTGTGCGC
sox9b	F	AGGTGCTGAAGGGCTACGACTGGT
	R	GATTTCCTCCGTCTGGGCTGGTATT
cxcl12b	F	CAAGTCATTGCCAAGCTGAAG
	R	CTCGTCTGTTTACTCTGAGCG
rdh10a	F	AGTTCACTGGGCCTTTTCAG
	R	ACACCAGCGTCATCTTGATAC
hoxb8a	F	ACAACTGTTCCCGTGGATG
	R	TGTGACACTTCAATCCGACG
rspo2	F	TCCAACCATCGCTGAATCTAG
	R	TCGCTGTGTTGGTTCTGAG
barx1	F	CCGGATCAGAAGGTATCAAGTC
	R	GGAAACTTCAGGATACCCGTC
b-actin	F	CGAGCAGGAGATGGGAACC
	R	CAACGGAAACGCTCATTGC
rdh10b	F	GAGAGCCATACTAACAGACCAG
	R	AGGGTACATGCACTTATCAGC

mRNA generation primer	5'--3'		
EcoRI-inhbaa-F	CG GAATTC AGTCCCAGACCTCTTACGAG		
XhoI-inhbaa-R	CTAACG CTCGAG ttacgagcagccgcattctt		
ECORI-sox9b-F	CG GAATTC ttataacacacacgcgtgcg		
XhoI-sox9b-R	CTAACG CTCGAG TCAGGGTCTGGACAGCTGTG		
BamHI-has2-F	CTG**GGATCC**ATGAGATGTGATAAAGCGGTCAGC		
XhoI-has2-R	GTCA**CTCGAG**CTATACGTCAAGAACCATGTC		

Table S1. PCR Primer Sequences Used in the Paper. Related to Figure 5 and Figure 6.

alpi.1
amer2
ets2
foxa3
g6pc3
gmpr
inhbaa
lama4
nog2
pecam1
pisd
pts
rtn4rl2a
slit1a
sox9b
spag1a
srl
trim69
tyr
zgc:153184

Table S2. Genes have hyper-DMR in 2 kb upstream and downstream of transcription start sites as well as transcriptional downregulation in *tet2/3^{DM}* hearts (fold change >2). Related to Figure 5.